INTERFERENCE MANAGEMENT IN WIRELESS LAN MESH NETWORKS USING FREE-SPACE OPTICAL LINKS

INTERFERENCE MANAGEMENT IN WIRELESS LAN MESH NETWORKS USING FREE-SPACE OPTICAL LINKS

BY

VALAVAN RAJAKUMAR, B. E. (ELECTRICAL & COMMUNICATION)

SEPTEMBER 2007

A THESIS

SUBMITTED TO THE DEPARTMENT OF ELECTRICAL AND COMPUTER ENGINEERING

AND THE COMMITTEE ON GRADUATE STUDIES

OF MCMASTER UNIVERSITY

IN PARTIAL FULFILLMENT OF THE REQUIREMENTS

FOR THE DEGREE OF

MASTER OF APPLIED SCIENCE

MCMASTER UNIVERSITY

MASTER OF APPLIED SCIENCE (2007) McMaster University

(Electrical and Computer Engineering) Hamilton, Ontario

TITLE: Interference Management in Wireless LAN Mesh Networks using Free-Space Optical Links

AUTHOR: Valavan Rajakumar, B. E. (Electrical & Communication)

SUPERVISOR: Dr. Terence D. Todd, Professor of Electrical and Computer Engineering, B.A.Sc., M.A.Sc., Ph.D. (University of Waterloo)

NUMBER OF PAGES: xii,88

Abstract

Wireless LAN mesh networks (WMNs) are a cost effective way of deploying wireless LAN (WLAN) coverage over extended areas. As WMNs become more populated, scalability issues may arise due to the co-channel interference which is inherent in publicly available RF (radio frequency) channels. This co-channel interference can severely degrade network capacity and link reliability and may eventually make it impossible to operate with the frequency channels for which the network was originally designed. In this thesis, this problem is addressed by selectively installing supplementary free-space optical (FSO) links when RF link performance has deteriorated. The frequency assignment problem is solved using a heuristic technique based on a genetic algorithm. In order to determine the quality of the results, the proposed algorithm is compared with a lower bound solution obtained using an Integer Linear Programming (ILP) formulation.

Another advantage of FSO links is that they may reduce node power consumption compared with conventional RF links. This may be an important consideration in cases where power consumption at the nodes is important, such as in solar powered mesh networks. Power consumption estimates of RF and FSO links are obtained and compared for different data rates. This data is then used along with historical solar

insolation data to estimate the solar panel and battery sizes required to guarantee a given node outage probability. The results show that no extra provisioning is required for replacing the deployed wireless nodes with new FSO links.

Acknowledgments

I would like to thank my supervisor, Dr. Terence D. Todd, for his valuable assistance and support during the course of this project. The depth of knowledge which he possessed helped me to gain a deeper insight into the subject. Apart from technical aspects, I also improved my technical writing skills. I would also like to express my sincere thanks to Dr. Sasthi C. Ghosh, Mohammad Smadi and Dr. Steve Hranilovic for their useful advice in various parts of this work. I wish to thank my fellow graduate students, Amir Sayegh, Vahid Azhari, Bin Wang, Min Shen, Ahmed Kholaif, Qiao Lu and Rafal Rzeczkowski who were very supportive and have always provided a friendly working atmosphere. I extend my heartfelt thanks to my parents and brother for their constant encouragement, motivation and love, and who were always there to share my joy and sorrow. Finally I thank and praise God, for giving me the spirit to face challenges in life and guiding me in right directions.

Contents

Abstract iii

Acknowledgments v

1 Introduction 1

1.1 Overview 1

1.2 Motivation 3

1.3 Organization of the Thesis 4

2 Wireless Mesh Networks 6

2.1 IEEE 802.11 Standard 6

2.1.1 IEEE 802.11 Networking 8

2.2 Wireless Mesh Networks 9

2.2.1 Advantages of WMN 9

2.2.2 Multi-Radio Mesh Networks 11

2.3 Power Saving in IEEE 802.11 and WMN 11

3 Free-Space Optics 13

3.1 Overview 13

3.2 Motivation for using FSO Links 14

3.3 Factors Affecting the Performance of FSO Links 15

3.3.1 Atmospheric Effects on FSO Links 15

3.4 Design Considerations and Safety Regulations 17

3.5 FSO Link Budget 19

3.5.1 Power Consumption Estimate 22

4 Frequency Assignment **24**

4.1 Overview 24

4.2 Background 25

4.3 Problem Formulation 26

4.4 NP-complete Proof of the Problem 28

4.5 Optimal Bound Formulation 31

4.6 RF Frequency and FSO Link Assignment using a Genetic Algorithm (GA) 32

4.7 Performance Results 40

4.7.1 Frequency Assignment for Grid Structures 40

4.7.2 Frequency Assignment for Grid Structures with External Interference 50

4.7.3 Frequency Assignment for Non-Grid Structures 53

4.7.4 Frequency Assignment for Non-Grid Structures with External Interference 55

5 Resource Allocation of FSO Solar Powered Nodes **63**

5.1 Overview 63

5.2 Background 65

5.2.1 Energy Flow Model 66

5.3 Power Consumption Estimates for RF and FSO Nodes 67

5.4 Simulation Method 71

5.5 Results 73

6 Conclusions **78**

Bibliography **81**

List of Tables

3.1 Visibility data for different cities ([55]) 18

3.2 Different classes of lasers [61] 19

3.3 Parameters for a short-range FSO link 20

3.4 Link budget for the FSO link 21

4.1 Threshold calculation B 41

4.2 No. of FSO links for different square grids (GA and ILP results) . . . 44

5.1 Minimum cost resource allocation of FSO nodes for different throughputs and a P_{out} of 10^{-2} (Phoenix) 74

5.2 Minimum cost resource allocation of RF nodes for different P_{out} values (Toronto) 74

5.3 Minimum cost resource allocation of FSO nodes for different P_{out} values (Toronto) 74

List of Figures

2.1 Wireless Mesh Network 10

3.1 Atmospheric effects on FSO links 18

3.2 A short-range FSO Link 22

4.1 Sample network and mapping of link interference matrix (G') 28

4.2 Mapping to maximum induced k-colorable subgrpah problem 30

4.3 (a) Example interference graph G' and (b)-(c) Two frequency assignment results 34

4.4 Partially matched crossover operation 36

4.5 Integer programming FSO link placement result for 4×4 mesh with 8 frequencies. (No. of FSO links = 6) 42

4.6 Genetic algorithm (optimal) FSO link placement result for 4×4 mesh with 8 frequencies. (No. of FSO links = 6) 42

4.7 Integer programming FSO link placement result for 5×5 mesh with 8 frequencies. (No. of FSO links = 10) 43

4.8 Genetic algorithm (non-optimal) FSO link placement result for 5×5 mesh with 8 frequencies. (No. of FSO links = 11) 43

4.9 Integer programming and genetic algorithm results for 4×4 mesh with varying number of frequencies 46

4.10 Integer programming and genetic algorithm results for 5×5 mesh with varying number of frequencies 46

4.11 Integer programming and genetic algorithm results for 6×6 mesh with varying number of frequencies 47

4.12 Genetic algorithm results for varying mesh sizes with 3 frequencies . 48

4.13 Genetic algorithm results for varying mesh sizes with 8 frequencies . 49

4.14 Genetic algorithm results for varying mesh sizes and frequencies for a data rate of 11 Mbps 49

4.15 Genetic algorithm results for varying mesh sizes and frequencies for a data rate of 54 Mbps 50

4.16 Percentage of FSO links in a grid for varying mesh sizes and frequencies for a data rate of 11 Mbps 51

4.17 Percentage of FSO links in a grid for varying mesh sizes and frequencies for a data rate of 54 Mbps 51

4.18 Frequency assignment results for 4×4 grid with external interfering APs 53

4.19 Frequency assignment results for 5×5 grid with two external frequencies overlapping in the top left region of grid 54

4.20 Non-grid structure AP placement (No. of APs=24, No. of links = 32) 56

4.21 Frequency assignment result for the non-grid structure with 3 frequencies (No. of FSO links=19, No. of RF links=12) 57

4.22 Frequency assignment result for the non-grid structure with 5 frequencies (No. of FSO links=13, No. of RF links=19) 58

4.23 Non-grid structure AP placement with interfering APs 60

4.24 Frequency assignment result for the non-grid structure with 3 frequencies and external interfering APs (No. of FSO links = 22, No. of RF links = 10) 61

4.25 Frequency assignment result for the non-grid structure with 5 frequencies and external interfering APs (No. of FSO links = 15, No. of RF links = 17) 62

5.1 A solar powered access point model 64

5.2 Power consumption values of FSO and RF links for different throughputs 71

5.3 Contour plot for different outage probabilities (Phoenix) 72

5.4 Contour plot for different outage probabilities (Toronto) 73

5.5 Minimum cost resource allocation results for different throughputs and a $P_{out} = 10^{-4}$ (Phoenix) 76

5.6 Minimum cost resource allocation results for different throughputs and a $P_{out} = 10^{-2}$ (Phoenix) 76

5.7 Minimum cost resource allocation results for different throughputs and a $P_{out} = 10^{-4}$ (Toronto) 77

5.8 Minimum cost resource allocation results for different throughputs and a $P_{out} = 10^{-2}$ (Toronto) 77

Chapter 1

Introduction

1.1 Overview

Mesh Networks consists of a collection of nodes providing user connectivity through multi-hop communication. WLAN (Wireless Local Area Networks) provides wireless connectivity to users and are governed by IEEE 802.11 standards. A WLAN mesh network (WMN) is a mesh network implemented over an IEEE 802.11 WLAN system. WMNs are becoming a cost effective way to deploy widespread wireless coverage in outdoor environments and metro-area hot-zones. These networks can be used to distribute excess bandwidth, thereby minimizing wired Internet connections and leased backhaul links, resulting in reduced installation and operating costs. They provide seamless connectivity and mobility to the users, which have resulted in their widespread deployment over the past few years.

Frequency assignment is the process of assigning frequencies to wireless links such that a minimum signal-to-noise ratio can be maintained for the links to operate at the designed capacity. In WLAN mesh networks, frequencies are usually assigned to links subject to an acceptable RF co-channel interference criterion, such as minimum signal-to-interference (SIR) ratio, which is the ratio of signal power at a given link to the co-channel interference power received at the same link. When a WLAN mesh is deployed, a frequency assignment is normally attempted such that all backhaul links can be simultaneously activated. Assignment frequencies can obviously be reused on multiple links but only subject to those links satisfying the desired SIR threshold. However, when RF interference becomes unacceptable in a deployed network, FSO (free-space optical) links can be used to replace one or more of the relay links (i.e., those which operate between WLAN mesh points) so that the backhaul network can function as configured originally.

In this thesis we address the co-channel interference in WMNs by selectively installing a limited number of FSO links when the throughput of the link deteriorates due to unacceptable radio frequency (RF) interference. Before the FSO links are deployed the system may operate in a degraded mode using a combination of link rate reduction and temporal scheduling to combat RF interference.

In order to make wireless networks ubiquitous and to exploit the full advantages of mesh networks, the issue of power provisioning in mesh nodes also needs to be addressed. Although mesh networks are able to provide a quick platform for establishing a communication network, they cannot be realized for all possible situations, since continuous node power connections may be very expensive. An alternative is to operate these mesh nodes using sustainable solar powered nodes. Using such a renewable source of energy, WLAN mesh nodes can be deployed quickly and inexpensively for outdoor networks. Nodes in such networks may have multiple WLAN radios which can be used for providing end station coverage and backhaul links. Wind power is also another renewable source of energy that can be used to satisfy power requirements for provisioning wireless nodes [52].

1.2 Motivation

Free space optical (FSO) communication has been gaining attention in recent years as an effective means for transmitting at high data rates over short distances. It provides unregulated bandwidth, low power consumption, secure communication, and interference free operation. Recent advances also show that such links can reliably operate over outdoor WLAN mesh node distances. FSO links are highly directional, but do not have the same omni-directional or antenna steering capabilities as RF links.

In this thesis, the usage of FSO links has been proposed to solve the interferece problem in WMN. The interfered RF links in an exsiting WMN are replaced by specially designed FSO links. In an existing WMN, it is desirable to minimize the number of FSO link replacements to be made since any modification to the network implies additional cost. The selective FSO installation problem is formulated with the objective of maximizing the number of simultaneously active RF links while satisfying interference constraints and minimizing the number of FSO links. The problem of joint frequency assignment and FSO link placement is shown to be an NP-complete problem under a cumulative RF interference constraint. An efficient heuristic is proposed which solves the channel assignment problem using genetic algorithms. In addition to the proposed heuristic, an integer linear programming formulation is used to obtain lower bounds for small network sizes. Our comparisons show that the proposed algorithm gives good results compared with the computed bounds. The presented results also give an indication of the value of FSO links in mitigating the interference problem. In the ensuing sections, we focus entirely on the point-to-point backhaul links used by the WMN to relay traffic between nodes. The cost estimates of building new solar powered mesh nodes with FSO relay links are also presented and compared with a network consisting of RF radios. The provisioning costs are estimated by statistical provisioning methods, which determine the solar panel and battery size required for a given outage probability.

1.3 Organization of the Thesis

The reminder of the thesis is organized as follows. In Chapter 2, background information on IEEE 802.11 and the concepts of WMNs are explained. A general overview of power saving in IEEE 802.11 terminals and access points is also provided.

In Chapter 3, Free-Space Optical links and their commercial applications are explained. The motivation behind preferring FSO links to combat interference in WMNs is also described in this chapter. Power budget calculations, using off-the-shelf components for a typical short-range FSO link, are performed. The estimates obtained are used along with the power consumption values of a typical wireless link to compare the costs of provisioning an FSO link and an RF link using solar powered mesh nodes.

In Chapter 4, the co-channel interference problem is formulated as an integer linear programming (ILP) problem and a lower bound solution is obtained. An alternative and efficient heuristic technique in the form of a Genetic Algorithm (GA) is also proposed. Results obtained using both methods are compared for regular grid structures and non-grid structures in the presence and absence of external interference.

Chapter 5 provides calculations for power estimates of an FSO link and an RF link operating at different throughput rates. The concepts behind statistical provisioning of a solar powered node and the energy flow model are explained in detail. Results for the cost estimates of provisioning an RF node and an FSO node are also compared in this chapter.

Chapter 6 presents conclusions and possible directions for future work.

Chapter 2

Wireless Mesh Networks

2.1 IEEE 802.11 Standard

IEEE 802.11 denotes the set of standards developed by the IEEE 802 Task Group. The aim of the IEEE 802.11 standard is to address wireless connectivity issues within a distance of 100-250m for indoor and short range applications. The details regarding physical devices, channel modulation and radio link variations are specified in the physical layer specifications. Initially, the physical layer standards were based on Direct Sequence Spread Spectrum (DSSS) and Frequency Hopping Spread Spectrum (FHSS) for RF links, and Infrared (IR) for optical links [7]. IEEE 802.11b based on DSSS provides bandwidths up to a maximum of 11 Mbps compared to FHSS and IR which can reach only up to 2 Mbps. Circuit complexity and cost of production were some of the factors in favor of IEEE 802.11b (DSSS) gaining popularity. Further enhancements by the group led to the creation of IEEE 802.11a and IEEE 802.11g using Orthogonal Frequency Division Multiplexing (OFDM).

The media access control (MAC) layer defines the sharing of channels between different users. IEEE 802.11 supports two channel contention schemes, namely, the Distributed Coordination Function (DCF) and the Point Coordination Function (PCF). DCF is based on Carrier Sense Multiple Access with Collision Avoidance (CSMA/CA) and is supported by all access points (AP). In order for a successful transmission the sender has to receive an ACK frame from the receiver. Since the propagation range for the transmitter may be different from that of the receiver, a collision-free transmission at the sender does not guarantee a collision-free reception at the receiver. In DCF, the transmitting station has to sense that the channel is idle before transmitting. If the channel is busy it waits for an exponential random back-off interval and then senses the channel again. If it is still busy the back-off interval period is doubled until it reaches a maximum value. If the channel is idle, data packets are transmitted and the back-off interval is decreased.

The Point Coordination Function (PCF) is based on a centralized scheme where the stations are polled by the AP for transmission opportunities. While DCF is the fundamental access mechanism and is mandatory, the PCF is optional and may not be supported in some devices. Since the PCF resolves contention based on a centralized approach, it can provide a contention-free frame transfer service. In the IEEE 802.11 standard, service advertisements, called *beacons*, are periodically broadcast by the AP. The time period between transmissions of successive beacons is called a *superframe*. PCF divides every superframe into two parts, a contention-free period (CFP) and a contention period (CP). In the CFP, an AP polls the end stations and grants them transmission opportunities. This period is then followed by a mandatory CP during which stations contend to access the channel based on the DCF access mechanism. The support of this CP is mandatory for all wireless devices working in the PCF mode in order to ensure the simultaneous co-existence of the DCF and PCF schemes.

2.1.1 IEEE 802.11 Networking

There are three wireless connectivity solutions mentioned in the IEEE 802.11 standard, namely the basic service set (BSS), the independent basic service set (IBSS), and the extended service set (ESS). The BSS consists of an AP connected to the wired network, which acts as a gateway to the Internet. Each mobile station (MS) has to associate itself with an AP. In this type of architecture, all the traffic goes through the AP, including the traffic between MSs.

In an IBSS wireless local area network (WLAN), the network consists of a group of MSs sharing the communication media on an ad-hoc basis. Coordination between the MSs enables them to communicate without any infrastructure. When several BSSs are connected, the entire set forms an ESS. One type of ESS network is a WMN, and the IEEE 802.11s group has been established to set up wireless mesh networking standards. Some of the major issues arising in such networking are link state discovery, negotiation with neighboring nodes, channel selection, interoperability between multiple-vendor solutions, routing, adaptability to dynamic changes in the network, security, and power saving [9].

2.2 Wireless Mesh Networks

Wireless mesh networking is a very active area of research that has recently been proposed and deployed in many places. Mesh networks can be divided into two main categories, those based on community area networks and those based on wireless mesh networks. Some examples of community networks are MIT Roofnet [1], Seattle Wireless [2] and the Southampton Open Wireless Network [4].

WMN consist of a collection of nodes working together to provide user connectivity, using multi-hop radio communication [51, 9]. WMNs have a hierarchical structure and they provide multi-hop relaying between APs to facilitate communication between the end users. A WMN primarily consists of mesh APs (MAPs) and mesh points (MPs). MAPs provide coverage to end stations and relay traffic to other MAPs and MPs. An MP is a relay node and does not provide coverage to the end users. Mesh networks are often self-healing [9], that is, if a node breaks down, the network can still operate, and as a result, the network is fault-tolerant to a great degree, providing a high degree of reliability. Mesh networks can be deployed in many topologies, such as full mesh, partial mesh, and round-robin mesh. Mesh networks differ from ad-hoc networks in that the individual nodes can connect to each other via multiple hops and are generally not mobile [53, 51]. A sample WMN is shown in Figure 2.1.

2.2.1 Advantages of WMN

WMNs have been widely used because they have three major advantages. First, they present the easiest connectivity solution to mobile users. They can be extended to

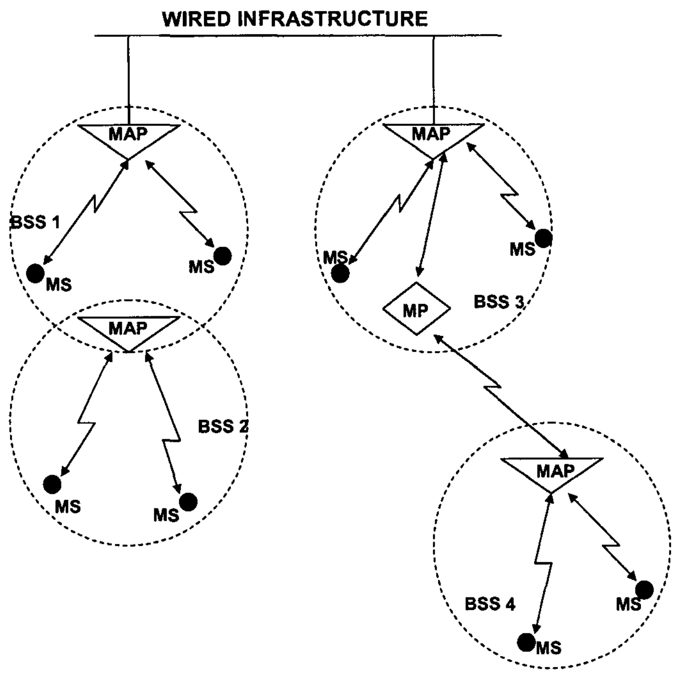

Figure 2.1: Wireless Mesh Network

provide coverage in outdoor areas, Wi-Fi hotspots, and busy areas, such as airports or railway stations where it may be practically impossible to lay cables or fiber optics. Mesh networks can also connect to different networks in a dynamic fashion, thereby rendering support systems to mission-critical applications. Second, they provide a cost-effective solution, as multiple BSS can be connected together and the overall coverage region can be expanded instead of having one large BSS. Third, WMNs offer flexibility and scalability. They can automatically detect new nodes, negotiate connection parameters, such as channel frequency, bandwidth, and modulation. All these advantages can be put in a nutshell as *self-configuring* and *self-healing* [9].

2.2.2 Multi-Radio Mesh Networks

Some deployment scenarios in WMNs can be satisfied with single-radio models while others may require multiple radios operating concurrently in order to satisfy traffic requirements. In a single-radio mesh architecture, both the user and relay traffic share a single radio. Recently, the development of WMNs using multiple radios has been gaining popularity due to the increased availability of inexpensive IEEE 802.11 interfaces. Multi-radio mesh networks are reliable and robust and provide path diversity against node and link failures. Overall, the throughput of the network can be improved with their increased capacity [30]. The frequency reuse factor is also improved using multiple radios. In this thesis, multiple-radio deployment is considered. Each node has at least two radio interfaces to a maximum of four radios towards the center of the grid.

2.3 Power Saving in IEEE 802.11 and WMN

Due to the limited energy reserves in mobile wireless devices, it is a desired characteristic to dissipate less power in wireless communication activities. IEEE 802.11 divides station activity into active mode and power saving (PS) mode. An MS in active mode can receive and send packets at any point in time. On the other hand, an MS in PS mode wakes up at periodic intervals to check for packets. APs transmit *beacon frames* at regular intervals and specify traffic indication map (TIM) bits for those PS hosts that have packets to be received. Once an MS is aware of its traffic indication status, it can receive the traffic by sending a PS-POLL in distributed co-ordination function (DCF) mode. In ad-hoc mode, a PS host wakes up periodically, and the wake-up period is denoted through an ad hoc traffic indication map (ATIM) window, which is assumed to be perfectly synchronized between the hosts. PS hosts contend by sending a beacon frame to occupy the time slot in order for the packets to be sent. IEEE 802.11 standard does not provide power saving mechanism at the APs, since it was considered that APs would always have infrastructure-based power supply. As a result, an AP is considered to be on all the time and only the MS which run on battery power could go into power-save mode.

The Wireless Networking Group at McMaster University has conducted extensive research on power saving in mesh networks. In [32], a power saving mesh architecture has been proposed based on extensions to IEEE 802.11e. An AP in PS mode uses a network allocation map (NAM) in its beacon broadcasts specifying the time of activity of the AP within the superframe. The AP remains idle during the inactive periods, and thus, it can save power. In [36], dynamic power saving methods have been proposed. One of the methods proposed was the use of forced AP power saving, where an AP can achieve the required power saving, irrespective of the network requirements with the help of NAM vectors in beacon broadcasts.

Chapter 3

Free-Space Optics

3.1 Overview

Free-space optical (FSO) links are point-to-point connections that transmit data by modulating the intensity of a LASER or light-emitting diode (LED) source. FSO links operate over the infrared range, and are currently used as solutions for "last mile problems" in outdoor situations, replacing short distance wireless links and optical fiber links. The importance of FSO links in providing wireless access has grown, particularly due to the limited wireless spectrum and increased co-channel and external RF interference. FSO links are interference-free in reference to neighboring FSO links because of the point-point nature of their connection. FSO links are preferred over fiber optic cables because of the extremely high installation cost, maintenance overheads, and power provisioning difficulties in busy and remote sites using fiber optics. In spite of these advantages, however, the performance of FSO links is limited by atmospheric and beam-spreading losses.

In the rest of the chapter, the motivation behind preferring FSO links to combat interference in WMN is explained. Details of some of the external (atmospheric) factors which affect the performance of FSO links are also provided. Power budget calculations for a short-range FSO link are performed using off-the-shelf components. The specifications for these components are also mentioned in Table 3.3.

3.2 Motivation for using FSO Links

FSO links are capable of high datarates and they offer theoretically unregulated bandwidth as the FSO transmission is only limited by the power emission (radiation exposure) limits. FSO circuits also consume very low power and may be an advantage in power provisioning using battery powered nodes. Due to their directional nature, FSO links provide protection against casual eavesdropping. Some of them are used in directed high speed relay networks, which use LASER diodes reaching up to a distance of 4km and providing bandwidths of about 155 Mbps [60]. FSO links cannot provide connectivity over long distances, as fiber optic cables can, or ubiquitous connectivity in non-LOS regions, unlike some wireless links. Therefore, FSO links are not a complete replacement for fiber optic and wireless links, but for short distance LOS communication they are often the best value in terms of cost and performance.

FSO links also satisfy the link availability requirements in enterprise markets which is about 99.9%. In this thesis, selective deployment of FSO links as a replacement for certain WLAN RF links is proposed. Since an FSO link is installed as a replacement for an interfered RF link, it is important to ensure that it can reliably provide data rates that are at least as high as the RF link. In addition, when the WLAN mesh nodes are battery operated (such as in a solar powered WLAN mesh [52, 29, 36]), it is also important that the power consumption of FSO links does not exceed that of the replaced RF link.

3.3 Factors Affecting the Performance of FSO Links

Many factors affect the performance of FSO links and can be split into [55] internal parameters and external parameters (atmospheric effects). Internal parameter variations are primarily caused by the properties of physical components used in the design of an FSO link. They include wavelength, LED output power, beam-spreading losses, transmitter and receiver losses and lens losses.

3.3.1 Atmospheric Effects on FSO Links

All of the above-mentioned design parameters can be controlled by an FSO provider or service provider. But the performance of FSO links depends mainly upon the climatic condition and the physical location of the installation. The stability of FSO links can be characterized by the visibility between the transmitter and the receiver. Visibility is defined here as the distance at which the intensity drops to 2% of its transmitted value. Some of the major factors that affect the Visibility, measured in km, are as follows.

1. <u>Fog</u>: Atmospheric attenuation is mainly due to fog. Fog affects the visibility of

FSO links and, hence, the operating range. Fog particles scatter the propagating light and the received signal power is reduced. FSO links cannot be operated during dense fog conditions as attenuation level is about 300dB/km (Table 3.3) and the light waves are affected by Mie scattering phenomenon. In the link budget calculations, FSO links are designed based on the attenuation caused by fog alone in Section 3.5, as there are well-defined preventive measures for some factors and the attenuation caused by other factors do not sufficiently affect the link margin.

2. Solar Interference: FSO links are based on light-wave technology and sunlight results in high levels of background radiation. Sunlight can cause severe problems if it falls directly within the field-of-view (FOV) of the receiver. Another possibility, apart from direct sunlight, is the reflection of sun rays by polished surfaces such as mirrors, window panes, etc. A photodetector at the receiver generates charges proportional to the amount of light incident on its surface. So excess sunlight within the FOV can exceed the maximum specified current limits for a photodetector. One of the methods to avoid this problem is to maintain the transmitter height lesser than that of the receiver, as the sunlight would not fall within the FOV of receiver [63].

3. Alignment Errors: FSO receivers generally have an acceptance region within which the transmitted light should be focused. Building motion can cause alignment errors and affect the FOV of an FSO receiver. Thermal variations cause bending of buildings, and are proportional to the height of the building.

Wider-beam transceiver and automatic tracking mechanisms can be used to avoid the alignment errors. High frequency base motion caused by huge machinery and the resistance of building materials to shocks caused by walking or regular motion are also some of the factors affecting FSO alignment [55].

4. Scintillation:

   Scintillation can be defined as the changing of light intensities in time and space at the plane of a receiver. The signal at the receiver varies because of pockets of refractive indices along the transmit path. The change in the refraction of the directed beam from the transmitter will result in the same effect as passing a light through a glass medium having a different refractive index. Overall, scintillation causes rapid fluctuations in the received signal strength. However, in most systems, when the transmission range is less than 1 km, there is enough dynamic range to compensate for scintillation effects [55]. Some solutions requiring high reliability are designed with multiple LASER transmitters, which reduce the probability of errors arising due to scintillation. Figure 3.1 illustrates the effects of atmosphere on the FSO links.

3.4 Design Considerations and Safety Regulations

FSO links can be designed using either LEDs or LASER diodes. Lasers present a potential risk when exposed to the skin or eyes and are known to cause injury, because of their coherent beams and very high intensities. However, not all kinds of LASER devices are dangerous in reference to eyes. Lasers, operating in wavelengths

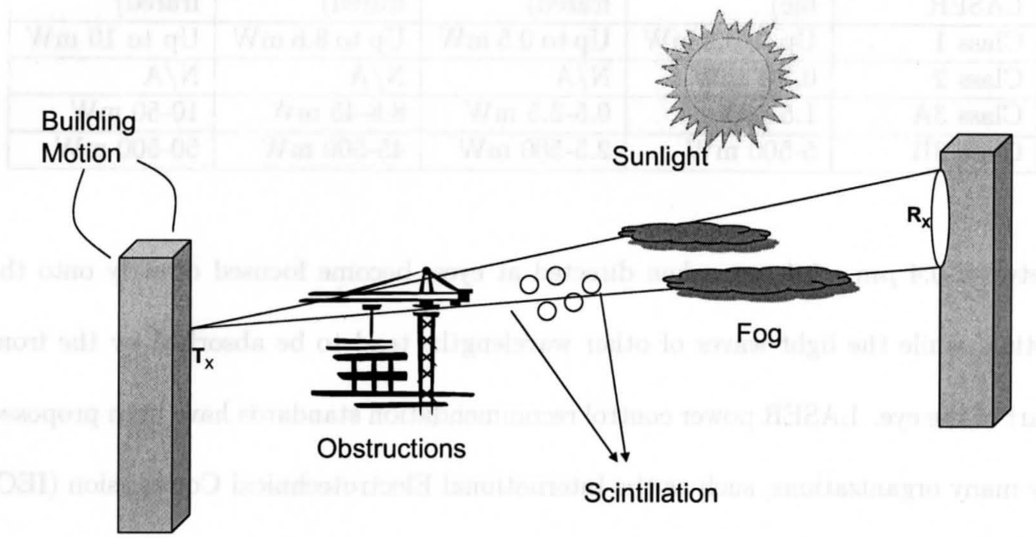

Figure 3.1: Atmospheric effects on FSO links

Table 3.1: Visibility data for different cities ([55])

Visibility (miles)	≥0.5	≥1	≥2	≥5	≥10
Los Angeles	98.4	97.2	93.7	76.3	49.3
Washington	99.6	99.1	97.6	87	61.8
Phoenix	99.9	99.9	99.9	99.5	98.1
Toronto	99.1	98.3	95.9	85.7	70.1
San Francisco	99.5	99.2	98.4	92.6	73.3
Tucson	100	100	99.9	99.8	99.4
New York	99.5	98.7	96.4	77.5	55.2

Table 3.2: Different classes of lasers [61]

Types of LASER	650 nm (visible)	880 nm (infrared)	1310 nm (infrared)	1550 nm (infrared)
Class 1	Up to 0.2 mW	Up to 0.5 mW	Up to 8.8 mW	Up to 10 mW
Class 2	0.2-1 mW	N/A	N/A	N/A
Class 3A	1.5 mW	0.5-2.5 mW	8.8-45 mW	10-50 mW
Class 3B	5-500 mW	2.5-500 mW	45-500 mW	50-500 mW

between 0.4 μm - 1.4 μm, when directed at eyes, become focused directly onto the retina, while the light waves of other wavelengths tend to be absorbed by the front part of the eye. LASER power control recommendation standards have been proposed by many organizations, such as the International Electrotechnical Commission (IEC) [65] , The American National Standards Institute (ANSI) [64]. Some of these are guidelines, while some are enforced by law. Warning signs, protective equipment, operating practices, and manual and automatic safety control systems have also been specified by these standardization bodies. The safe radiation exposure limits that have been specified by these bodies are referred to by the term Maximum Permissible Exposures (MPE's). Table 3.2 provides four primary categories of lasers, based on their wavelengths and MPEs.

3.5 FSO Link Budget

In this section, a link budget analysis is presented for a 155 Mbps FSO link over 200 m, which has significant link margin for these short-ranges. The power consumption of this FSO link is estimated using off-the-shelf commercial components. The design parameters chosen for the FSO link are summarized in Table 3.3. In our case, FSO

Table 3.3: Parameters for a short-range FSO link

Data Rate		155 Mbps
Link Distance	L	200 m
Beam Divergence	θ_b	10 mrad
Average Transmitted Power	P_t	10 mW
Rx. Aperture Diameter	D_r	0.10 m
Tx. Aperture Diameter	D_t	0.07 m
Wavelength	λ	850 nm
Bit-error rate		10^{-6}
Input referred noise	i_n	14 nA
Responsivity	R	0.6 A/W
Extinction Ratio	r_e	10
Sensitivity		-38.7 dBm

links have to replace some interfered RF links. The circuits should consume the least power possible, as they may be powered by battery-powered nodes.

The link design is based on an LED emitter since such units are less expensive, more robust, and have greater eye-safety compared to LASER emitters [42]. Due to cost constraints, it is assumed that the FSO link does not have any active tracking mechanisms to combat misalignment errors. As a result, the beam divergence is set to be wide compared to that of commercial units, $\theta_b = 10$ mrad. The average transmitted optical power and aperture sizes are below the eye-safe limits. The system is set to operate at $\lambda = 850$ nm since inexpensive silicon emitters and detectors exist at this wavelength.

The sensitivity of the receiver is the power required at the input of the receiver in order to provide a BER $= 10^{-6}$. In this case, the sensitivity in Table 3.3 is computed as,

$$\text{Sensitivity} = 10\log_{10}\left(\frac{4.75 i_n (r_e + 1)}{R(r_e - 1)} \times 10^3\right) \qquad [\text{dBm}] \tag{3.1}$$

Table 3.4: Link budget for the FSO link

System Losses		**Atmospheric Losses: L_a**			**Link Margin**
		Condition	Visibility	Attenuation (σ)	
Geometric loss (L_g)	-26 dB	Very Clear	20 km	0.48 dB/km	17 dB
Fading loss (L_f)	-2 dB	Clear	10 km	0.96 dB/km	17 dB
Misalignment loss (L_m)	0 dB	Haze	4 km	2.8 dB/km	16 dB
Optical Losses (L_o)	-3 dB	Light Fog	1 km	13 dB/km	15 dB
		Med. Fog	0.5 km	28 dB/km	12 dB
		Dense Fog	0.2 km	73 dB/km	3 dB
		Deep Fog	0.05 km	309 dB/km	**-44 dB**

where the responsivity, R, and input referred noise are taken from commercial components [45, 44].

The losses inherent in the channel are due to the losses in propagation, atmospheric losses, as well as system losses, and are summarized in Table 3.4. The received power can be written as,

$$P_r = L_f L_m L_o \underbrace{\frac{D_r^2}{(D_t + L\theta_b)^2}}_{L_g} \underbrace{e^{-\sigma L}}_{L_a} \tag{3.2}$$

where L_f, L_m, L_o and σ are listed in Table 3.4. Due to the large beam divergence, L_m is assumed to be negligible, while conventional values for L_o and L_f losses are used [55]. The geometric loss, L_g, is dominated by the wide beam width emitter used to ease pointing restrictions. The atmospheric loss, L_a, is calculated using the Beer-Lambert law, where the attenuation σ is calculated from an empirical fit to experimental data based on the visibility [41, Eqn.6].

The link margin specifies the extent to which P_r exceeds the minimum required sensitivity to ensure a reliable link. Notice that, according to Table 3.4, a significant link margin exists in all weather conditions except for the worst case attenuation experienced during deep fog. The reliability of the link will then depend on the relative

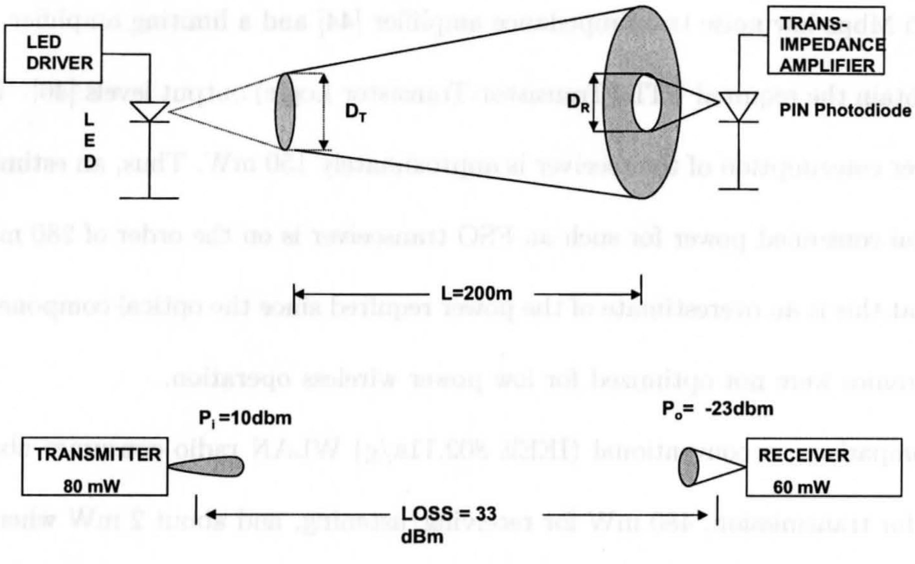

Figure 3.2: A short-range FSO Link

frequency of different weather conditions. A recent study using historic weather data for a variety of world cities over a period of 16 years, estimated that, for ranges on the order of 200 m, a 155 Mbps FSO link was able to maintain a reliable link with an availability of 99.99% [55, Table 6]. Thus, for the short ranges considered in this thesis, FSO links provide a significant link margin.

3.5.1 Power Consumption Estimate

In order to estimate the power consumption of the transmitter and receiver, commercial components designed for a 155 Mbps fiber link were employed. The combination of a commercial high-speed LED for communication applications [42] and a 155 Mbps LED driver [43] is able to output the required 10 mW optical signal at a total power consumption of approximately 130 mW. At the receiver, a high-speed photodiode [45], a 155 Mbps low noise transimpedance amplifier [44] and a limiting amplifier are used to obtain the required TTL (Transistor-Transistor Logic) output levels [46]. The total power consumption of the receiver is approximately 150 mW. Thus, an estimate of the total consumed power for such an FSO transceiver is on the order of 280 mW. Notice that this is an overestimate of the power required since the optical components and electronics were not optimized for low power wireless operation.

By comparison, a conventional (IEEE 802.11a/g) WLAN radio consumes about 780 mW for transmission, 480 mW for receiving/listening, and about 2 mW when in power save mode[36]. An RF link operates in half-duplex at a maximum data rate of 54 Mbps. If a given RF link is 100% utilized and transmitting in one direction, a replacement FSO link can provide about three times more data rate (155 Mbps), and is also bi-directional. It can easily be seen that the power consumption of the FSO link is always strictly less than the RF link regardless of its transmit/receive activity. Power consumption estimates and provisioning cost calculations of RF and FSO links are discussed in Chapter 5.

Chapter 4

Frequency Assignment

4.1 Overview

Frequency channels are assigned in wireless LAN mesh networks subject to strict co-channel interference constraints. Since the Wi-Fi frequency spectrum can be freely used by anyone, the co-channel interference in a network may increase after it is planned and deployed. In this chapter, selective placement of free-space optical (FSO) links is proposed when an RF link cannot satisfy its interference constraints. FSO links are highly directional and can combat the interference caused by RF links. The proposed solution methodology tries to allocate RF frequencies to a maximum number of links subject to interference constraints, and assign FSO links to the rest. As the replacement of interfered RF links with FSO links are carried to an already deployed network, replacement costs are extra overhead involved in maintaining an existing network. Hence, it is desirable to minimize the number of FSO links to be deployed. The RF frequency assignment problem is mapped as an instance of the maximum k-colorable induced sub-graph problem and hence, the NP-complete nature of the problem is proven. Since the problem is NP-complete, a heuristic technique based on a genetic algorithm is proposed and compared with the lower bound ILP solutions. The results obtained using both the proposed methods are compared. The proposed methods are extended to provide frequency assignment solutions in the presence of external interfering APs, and also for non-grid structures.

4.2 Background

There are many factors affecting the capacity of wireless mesh networks including end-user mobility, routing, media access control protocol, communication range and network topology. Reference [10] provides theoretic bounds on the throughput of wireless mesh networks and shows that the throughput of each node diminishes to zero as the number of nodes increases. In [11] an experimental test bed was used to show that a routing algorithm can select better paths by taking the quality of the wireless links into account rather than selecting paths using minimum hop counts. In [15], adaptive antenna arrays were used in mesh networks using the IEEE 802.11 DCF. It was shown that in many cases the transmitted power can be significantly reduced while still maintaining a sufficient link margin. This method of interference reduction by reducing the transmitted power is a key factor in improving capacity. In [16], a media access control protocol was proposed that accommodates the active nullifying of co-channel interferers which may arise during the course of ongoing transmissions. The work in [17, 20, 19] considered the use of non-overlapping frequency channels in multi-hop mobile ad-hoc networks. In [22], the channel assignment problem was addressed by minimizing interference from neighboring nodes. The work classified neighboring nodes as either interfering or not (a binary interference model) and the problem was solved using a Tabu search procedure. A binary interference model represents an ideal case, whereas, a cumulative interference model is more common in practice. In [18], a joint channel assignment and routing problem was formulated, taking into account interference constraints, the number of channels and the number of radios available at each mesh point. In [21], a mesh architecture was proposed that combines spatial separation using directional antennas and frequency separation using different channels.

4.3 Problem Formulation

In this section, the joint RF assignment FSO link placement problem is formulated as a graph coloring problem. Let us consider a multi-channel WMN of N mesh APs. It can be represented as a *reachability graph* $G = (N, E)$ where each AP will represent a node in G and two nodes have an edge (link) between them if they are within communication range. The communication range of each AP is equal and all links are bi-directional.

Let $K = \{1, 2, \cdots, k\}$ denote the given set of RF frequencies. It is assumed that the $E \times E$ interference matrix $C = (c_{ij})$ is known where $c_{ij} \geq 0$ indicates the (measured) interference that is caused on link i, if it operates on the same radio frequency, $f \in K$, as in link j. The interference matrix C is also a symmetric matrix

$c_{ij} = c_{ji}$. A radio frequency, $f \in K$, can be assigned to a link i if and only if the total cumulative co-channel interference due to other links' usage of the same frequency, $f \in K$, is below a pre-defined threshold B. Note that depending on the value of k and B, it may or may not be possible to assign a frequency to every link in G satisfying the cumulative interference constraint. When k is not sufficiently large, an FSO link is placed on each of the remaining links in G where a radio frequency has not been assigned. Note that FSO links are point-to-point and they do not interfere with any of the assigned RF channels. The objective is to assign the available RF channels in such a way that a minimum number of FSO link replacements are required, to avoid replacement costs to an existing network. In other words, given the reachability graph and a set $K = \{1, 2, \cdots, k\}$ of radio frequencies, the objective is to maximize the number of links that can be assigned to a given number of RF frequencies subject to satisfying the interference constraints.

The interference constraints can be represented by means of edge weights on an *interference graph* $G' = (N', E')$ which can be derived from the reachability graph G as follows. Each link in G will represent a node in G' and every pair of nodes i and j in G' has an edge between them with weight c_{ij}. The term c_{ij} denotes the interference between the nodes i and j and it is shown in the Figure 4.1.

Now, the above channel assignment problem can be modeled as a vertex coloring problem as follows. Given an undirected graph $G' = (N', E')$ with edge weight c_{ij} for every edge $(ij) \in E'$, the interference threshold B, and the set of available radio frequencies $K = \{1, 2, \cdots, k\}$, the graph theoretic problem is to find a coloring function t such that the maximum number of vertices of G' can be colored with k

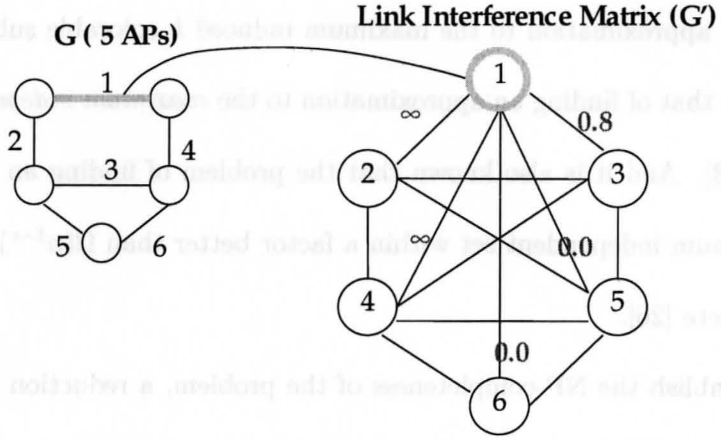

Figure 4.1: Sample network and mapping of link interference matrix (G')

different colors subject to

$$\forall i \in N', \quad W(i) = \sum_{j \in N' : t(i)=t(j) : j \neq i} c_{ij} < B. \tag{4.1}$$

where $W(i)$ denotes the total co-channel interference at a given node i. Note that constraint 4.1 ensures that the total co-channel interference $W(i)$ is below the threshold B.

4.4 NP-complete Proof of the Problem

A graph $T = (P, Q)$ is k-colorable if there exists a coloring of the vertices of T with k colors such that adjacent vertices are not colored using the same color. It is well known that deciding if a given graph is k-colorable is NP-complete [12]. Given a graph $T = (P, Q)$, the *maximum induced k-colorable subgraph* problem finds a k-colorable subgraph of T with maximum number of vertices. It is well known that finding an approximation to the maximum induced k-colorable subgraph problem is as hard as that of finding an approximation to the *maximum independent set*, for any fixed k [13]. And it is also known that the problem of finding an approximation to the maximum independent set within a factor better than $\Omega(n^{1-\epsilon})$, for any $\epsilon > 0$, is NP-complete [26].

To establish the NP-completeness of the problem, a reduction from an arbitrary instance of the *maximum induced k-colorable subgraph* problem on $T = (P, Q)$ to a coloring problem on $G' = (N', E')$ is used where k is the available number of *RF* channels. Define $N' = P$ and $E' = Q \cup R$, where R is the set of edges required to make G' a complete graph. Now consider the following weight assignment function $s : Q \longrightarrow B'(B + \epsilon)$ and $s' : R \longrightarrow 0$ which assigns each edge $e \in E'$ a weight equal to B' or 0 depending on whether $e \in Q$ or $e \in R$, respectively, as shown in Figure 4.2 for a given link i. Similarly the weight assignment function gives weight B' to each of the edges interfering with a given link and 0 to a non-interfering link. Note that T with weight B' on every edge remains as a subgraph of the graph G'. Clearly, if there exists a polynomial algorithm for solving the coloring problem on G' optimally, it will also result in a maximum induced k-colorable subgraph of T. This can be explained as follows. As the weights of each edge in Q is B', no vertex can be adjacent to a vertex of its same color in T in any optimal coloring on G' as the interference constraint in Equation 4.1 will be violated. Even if there exists one vertex u with an adjacent vertex of the same color, the cumulative co-channel interference $W(u)$ in

Equation 4.1 at the vertex u will be equal to B'. Hence this optimal coloring is also an optimal result for the maximum induced k-colorable subgraph problem on T. Thus the hardness results follows from the hardness of the maximum induced k-colorable subgraph problem.

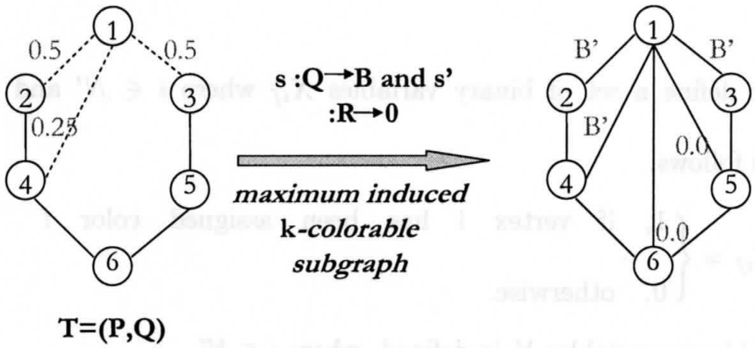

Figure 4.2: Mapping to maximum induced k-colorable subgrpah problem

Because of the NP-complete nature of the problem, a heuristic algorithm is required to solve it. In order to compare the performance of a proposed heuristic, a lower bound calculation is performed in the next section using an Integer Linear Programming (ILP) formulation.

4.5 Optimal Bound Formulation

The objective of the formulation is to maximize the number of vertices of G' that can be colored with k colors satisfying the interference constraints. The problem is formulated as an Integer Linear Programming (ILP) optimization. This calculation will give us a lower bound so as to compare the quality of results obtained by the proposed heuristic, but is only feasible for small problem sizes (upto 6×6 grid, which has 60 links).

Let us first define a set of binary variables X_{if} where $i \in N'$ and $f \in K = \{1, 2, \cdots, k\}$ as follows.

$$X_{if} = \begin{cases} 1, & \text{if vertex i has been assigned color f} \\ 0, & \text{otherwise.} \end{cases}$$

Another set of binary variables Y_i ie defined, where $i \in N'$.

$$Y_i = \begin{cases} 1, & \text{if } \sum_{f \in K} X_{if} = 1 \quad \text{(vertex i has been colored)} \\ 0, & \text{if } \sum_{f \in K} X_{if} = 0 \quad \text{(vertex i has not been colored).} \end{cases}$$

Let M be a large value greater than $\sum_{(i,j) \in E'} c_{ij}$. Now the objective is to

$$\max \sum_{i \in N'} Y_i,$$

subject to the following constraints,

$$\forall i \in N', \quad Y_i - \sum_{f \in K} X_{if} = 0 \tag{4.2}$$

and

$$\forall i \in N', f \in K, \quad \sum_{j \in N': j \neq i} c_{ij} X_{jf} \leq B X_{if} + (1 - X_{if}) M \tag{4.3}$$

Constraint 4.2 ensures that each vertex will be assigned at most one color. Constraint 4.3 makes sure that channel, f, is only assigned to vertex i when the cumulative co-channel interference due to other vertices' usage of the same channel is below the pre-defined threshold, B. The number of binary variables in this model is $|N'|k + |N'|$ and the number of constraints is also equal to $|N'|k + |N'|$. The heuristic method is proposed in Section 4.6 and the results are compared in Section 4.7

4.6 RF Frequency and FSO Link Assignment using a Genetic Algorithm (GA)

In this section, the genetic algorithm formulation for solving the joint frequency and FSO link assignment problem is proposed. When solving a problem using a genetic algorithm, it is required that the parameter set be coded as a finite-length string (or chromosome) over a finite alphabet [28]. A string S is assigned a fitness value using an appropriate fitness function. A collection of M (finite) such strings is called a population. A simple genetic algorithm is composed of three basic operators, (i) reproduction or selection, (ii) crossover and (iii) mutation [28].

Frequency assignment is performed on the link ordering (string) generated by genetic algorithm (GA) using a fitness function. Link ordering is the specific order in which the links are traversed and allocated frequencies from the given set of frequencies subject to interference criteria. A different link ordering of the same network graph will produce a different fitness value. Link ordering determines the quality of GA results. It is very important to try the GA on as many link orderings as possible to obtain one of the optimal solutions. Frequency channels are assigned to the nodes of the *interference graph* G' in a specific order and a node will be assigned the channel corresponding to the smallest integer in $K = \{1, 2, \cdots, k\}$, if the cumulative co-channel interference at all the previously assigned nodes including the node itself is satisfied.

Consider the following example shown in Figure 4.3. Figure 4.3(a) shows an interference graph G' with 5 nodes $a_1, a_2, \cdots, a_5$ and let $K = \{0, 1\}$ be the set of RF frequencies. The edges of the graph G' are labeled with weights according to the interference constraints as specified by $C = (c_{ij})$, i.e., the label α on the edge between a_i and a_j indicates the interference that will be caused if both the nodes a_i and a_j are assigned the same channel. Let the interference threshold be 0.18 in this example. The label $[\alpha]$ associated with each node of the graph G' of Figures 4.3 (b) and (c) indicate that the frequency channel $\alpha \in K$ is assigned to that node. Now, if the channels are assigned to nodes in the order $(a_1, a_3, a_2, a_5, a_4)$, as shown in Figure 4.3 (b), the number of required FSO links will be one. But if the channels are assigned to nodes in the order $(a_1, a_2, a_5, a_3, a_4)$, as shown in Figure 4.3 (c), the number of FSO links required will be zero.

It is clear from the above example that the ordering of the nodes has a strong impact on the required number of FSO links. Suppose there are N' nodes in G', the nodes can be ordered in $N'!$ ways and hence for sufficiently large N', it is impractical to find the best ordering by an exhaustive search. Instead, the genetic algorithm (GA) approach is used to find an optimal or near-optimal solution to the problem. Some of the basic terminology used in GA are :

1. Reproduction or Selection: It is defined as the process of replicating copies of potential strings from an existing population to a new population. A fitness

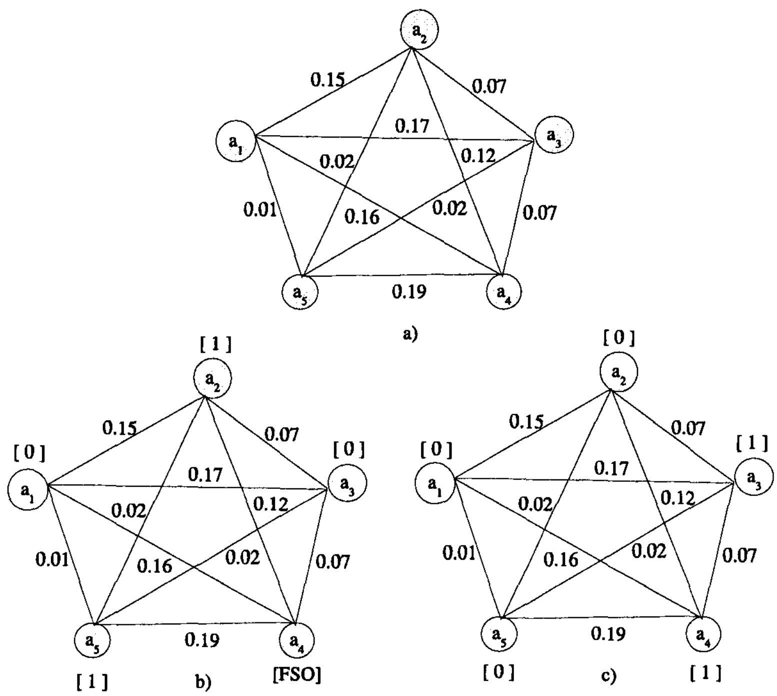

Figure 4.3: (a) Example interference graph G' and (b)-(c) Two frequency assignment results

function is used to evaluate the potential of a string and in the proposed algorithm, returns the number of FSO links required for a given network topology. A string has higher fitness value if it returns a minimum number of FSO links. A string S_i has more potential than the string S_j if $Fitness(S_i) > Fitness(S_j)$. Given a string (link ordering), the proposed fitness function in Algorithm 4.6 returns the number of links, which have been assigned RF frequencies. The strategy for selecting a potential string is similar to that used in [22]. Once the fitness values of the existing population are obtained, they are converted into probabilities and their cumulative distribution is used to create new strings for the next generation. The probability value of any given string appearing in the next generation is its fitness value divided by the sum over all the fitness values, which is given in the following equation,

$$p_i = \frac{fitness\_value(i)}{\sum_{j=1}^{N'} fitness\_value(j)} \quad . \tag{4.4}$$

This method tries to generate more strings from those that have high fitness values for the next generation. Also it does not completely eliminate the population with lesser fitness value, thereby trying to keep a balance. A string that may not yield a high fitness value after a few generations could yield a very good fitness value.

2. Crossover: In this operation, $M/2$ pairs are formed from the M existing strings in the current population. For each pair of strings a matching section is randomly defined and is used to effect a cross by performing a position-by-position exchange operation. This results in the generation of two new offspring's for the

next generation. Only some of the strings are subject to the crossover operation, decided based on the crossover probability. If a string is subject to the crossover operation, then a cross-over point is generated over the two strings and alternately swapped with the other. This crossover operator is commonly known as a Partially Matched Crossover (PMX) [28]. Figure 4.4 shows the difference between regular crossover and PMX. Figure 4.4(a) shows two strings which will undergo crossover operation. Figure 4.4(b) shows the results of regular crossover operation resulting in non-unique characters in strings, highlighted in bold font, while Figure 4.4(c) shows how the PMX is performed. Figure 4.4(d) shows strings that have unique characters as a result of PMX operation.

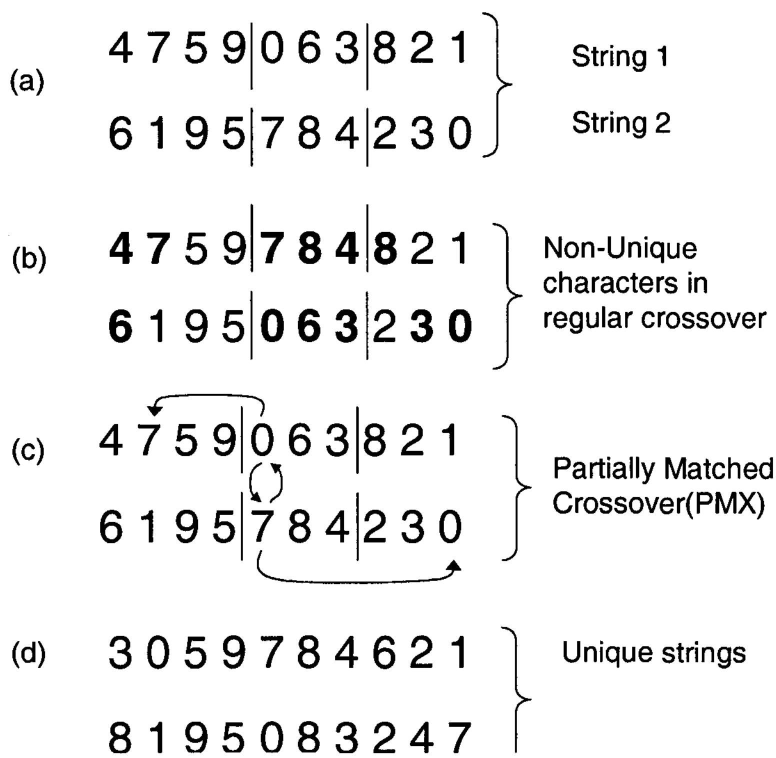

Figure 4.4: Partially matched crossover operation

3. Mutation: Mutation involves generating a random variable for each alphabet in a given string and this random variable denotes if a particular alphabet is to be altered. Mutation helps in avoiding the effect of local minima where the population of successive generations become too similar.

The genetic algorithm starts with an initial population (randomly generated) and in each iteration, a new (hopefully improved) population of the same size is generated from the current population applying the above mentioned three operators. Let S_b be the best string (with respect to the fitness value) of the population generated up to iteration t. In the elitist model of genetic algorithm (EGA), if S_b or any string better than S_b is not in the population generated in iteration $(t+1)$, then include S_b in the $(t+1)$-th population [28]. This technique is applied for solving the joint frequency assignment and FSO link deployment problem which ensures that successive iterations does not produce a worse population than the previous iteration.

The steps in the genetic algorithm are as follows,

1. The initial population is fixed as N=100.
2. The number of generations is set to a maximum of $G_{max} = 5000$.
3. The crossover probability is set as $P_c = 0.95$.
4. The mutation probability is set as $P_m = 0.95$.
5. Initial generation is set as $G = 0$.
6. Repeat steps (7-10) until $G < G_{max}$.

7. Initial population of 100 strings is selected randomly.

8. Fitness of each string is computed using Fitness function.

9. Selection of strings for the next generation is performed.

10. This population is subjected to crossover and mutation operations.

The genetic algorithm has been set a crossover probability of 0.95 and a mutation probability 0.95. A high crossover and mutation probability avoids the effect of local minima and tries to generate as many new strings as possible. As the EGA model is used in the simulations, the best possible solution is always tracked and propagated in successive iterations, and it allows more freedom to search through many possible solutions.

The genetic algorithm is applied to the *interference graph* $G' = (N', E')$, where the interference constraints given by the matrix $C = (c_{ij})$ as described in Section 4.3. Let us consider a random order of the nodes in N' as a string S or chromosome. The fitness $Fit(S)$ of a string S used in the algorithm is described by the following function, which returns the number of RF links required if frequencies are assigned to nodes of G' following the order as specified by S. The objective here is to find a string for which the fitness value is as high as possible.

Algorithm 1 function $Fit(S)$

1: **begin**

2: $t[1] \leftarrow 1$

3: // $t[i]$ is the frequency assigned to *nodei* (i-th node of S)

$No\_of\_FSO \leftarrow 0$;
for $i = 2$ to $|N'|$ **do**
  for $f = 1$ to k **do**
    $t[i] \leftarrow f$
    for $j = 1$ to i **do**
      if $t[j] = f$ **then**
        if $W(j) = \sum_{p \in \{1,2,\cdots,i\}; t[p]=f; p \neq j} c_{jp} < \mathrm{B}$ **then**
          $allotment \leftarrow yes$
        else
          $allotment \leftarrow No$
          $break$
        end if
      end if
    end for
  end for
  if $allotment = No$ **then**
    $t[i] \leftarrow fso\_link$
    $No\_of\_FSO + +$;
  end if
end for
return $|N'| - No\_of\_FSO$
end

Another important constraint stated in [22] is that an elitist genetic algorithm model converges to the global optimal solution with any choice of initial population as the number of iterations goes to infinity. It is also stated that no finite stopping time can guarantee an optimal solution. In the simulations performed the process is terminated after a fixed number of iterations.

4.7 Performance Results

4.7.1 Frequency Assignment for Grid Structures

In this section the results of the genetic algorithm and the integer programming formulation are compared for small mesh sizes. Since the number of links(N) for mesh sizes greater than 7×7 increase significantly, the number of binary variables required to be solved in the ILP also increase. The search space and time increase (2^N) exponentially and hence the results are obtained using GA alone. The SIR values corresponding to the IEEE 802.11 data rates of 1 Mbps, 11 Mbps and 54 Mbps are used in calculating the interference threshold (B). The number of frequencies is varied from 3, which is number of non-overlapping frequencies in IEEE 802.11b ,up to 8 and a Piecewise-Linear Exponential Path-Loss Model is used for the simulations. The path loss exponent is 2.8 upto 500 m distance and 4.5 after 500 m. The minimum SIR value for a given datarate, denoted by $MinSNR(datarate)$ is obtained from cisco aironet AP datasheet [3]. The interference factor is calculated based on the formula in Equation 4.5.

$$Interference\, threshold\ (B) = \frac{Pathloss}{MinSNR(datarate)} \tag{4.5}$$

Table 4.1: Threshold calculation B

Data rate	Threshold
1	1.0000
11	0.03852
54	114.815

where,

$$Path\ loss = \frac{1}{d^{\alpha}} \tag{4.6}$$

where, $d = 200m$ and $\alpha = 2.8$. The results are shown in the Table 4.1.

The GA results and the optimal ILP results, denoting the number of FSO links required for square meshes of sizes 4, 5 and 6 are shown in Table 4.2. The frequency assignment results obtained by the ILP and GA are also shown for two cases, one for which the GA produces optimal results and another for which it is non-optimal. The FSO placement results of ILP in Figure 4.5 and the GA in Figure 4.6 are examples for a 4×4 mesh with 8 frequencies. In the above case the GA provides optimal results, although the placement results are different from that of the ILP results. The GA frequency assignment result in Figure 4.8 for a 5×5 mesh with 8 frequencies are non-optimal compared to ILP results in Figure 4.7, but it varies by 1 link from the optimal solution. It can be observed that both the ILP and GA try to allocate FSO links in the center of the mesh as the center link interfere with more number of links rather than the links towards the edges.

The comparison in Table 4.2 and in Figures 4.9, 4.10 and 4.11 shows the number of FSO links required for square meshes of sizes 4, 5 and 6 . For a 4×4 mesh, the results exactly match. The genetic algorithm often gives optimal results in very few

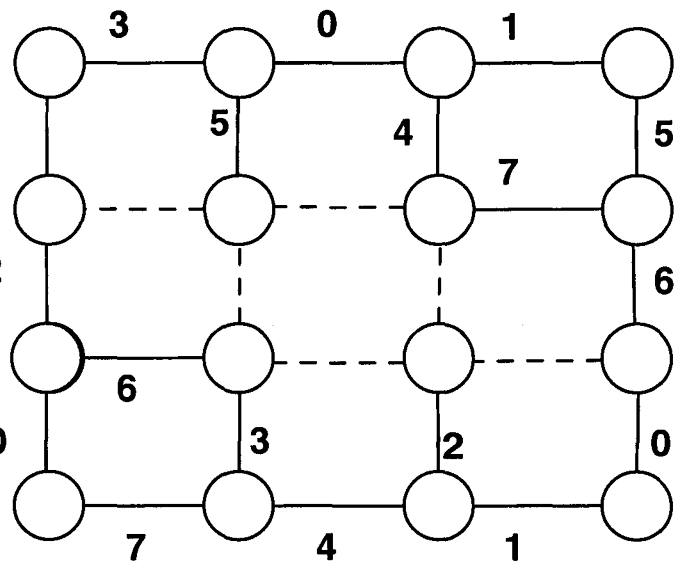

Figure 4.5: Integer programming FSO link placement result for 4 × 4 mesh with 8 frequencies. (No. of FSO links = 6)

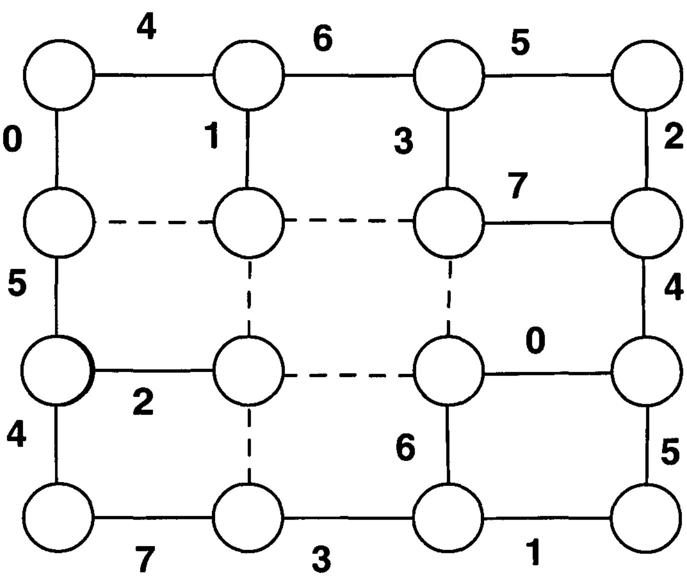

Figure 4.6: Genetic algorithm (optimal) FSO link placement result for 4 × 4 mesh with 8 frequencies. (No. of FSO links = 6)

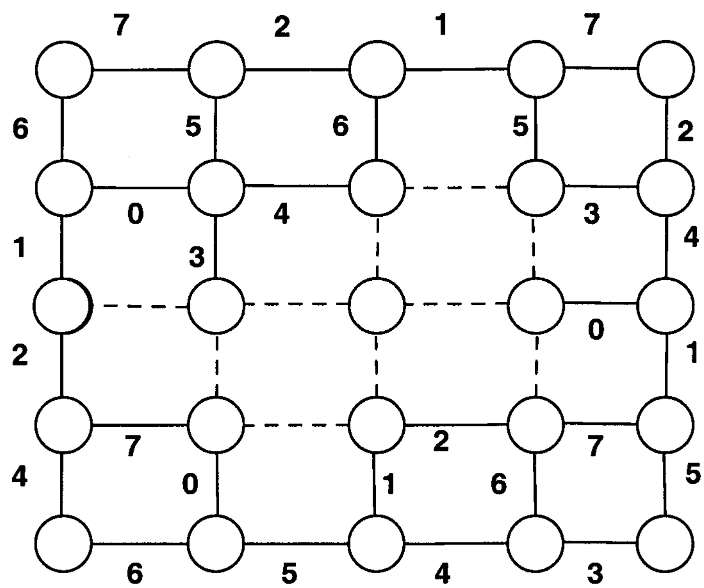

Figure 4.7: Integer programming FSO link placement result for 5 × 5 mesh with 8 frequencies. (No. of FSO links = 10)

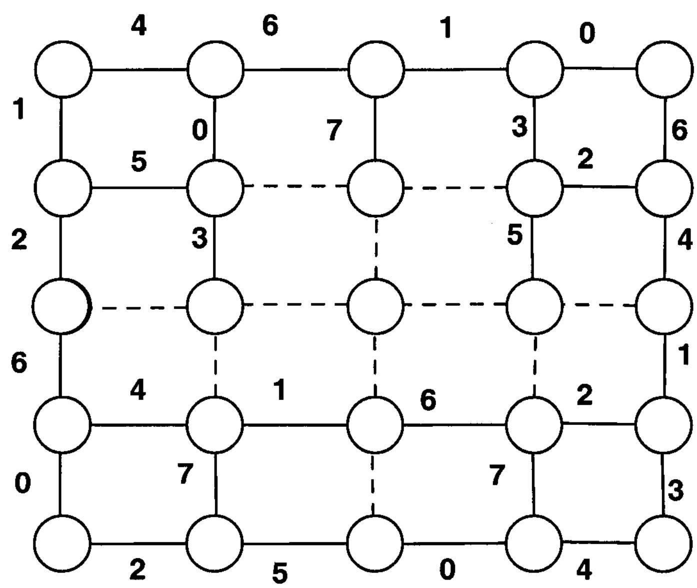

Figure 4.8: Genetic algorithm (non-optimal) FSO link placement result for 5×5 mesh with 8 frequencies. (No. of FSO links = 11)

Table 4.2: No. of FSO links for different square grids (GA and ILP results)

4 × 4 Mesh				
No. of Frequencies	ILP results (11 Mbps)	GA results (11 Mbps)	ILP results (54 Mbps)	GA results (54 Mbps)
3	15	15	18	18
4	12	12	16	16
5	11	11	14	14
6	9	9	12	12
7	8	8	11	11
8	6	6	10	10
5 × 5 Mesh				
No. of Frequencies	ILP results (11 Mbps)	GA results (11 Mbps)	ILP results (54 Mbps)	GA results (54 Mbps)
3	28	28	29	29
4	24	24	26	26
5	20	20	23	24
6	16	16	20	21
7	13	13	18	19
8	10	11	16	16
6 × 6 Mesh				
No. of Frequencies	ILP results (11 Mbps)	GA results (11 Mbps)	ILP results (54 Mbps)	GA results (54 Mbps)
3	42	43	48	48
4	37	38	44	44
5	32	34	40	40
6	28	29	36	36
7	23	25	32	32
8	20	21	28	29

iterations, because of two possible reasons. One is the symmetric structure of 4×4 and the other is the small number of link orderings. When the results are observed for the 5×5 mesh in Figure 4.10, the number of required FSO links obtained using GA differ by at most 1 from that of the ILP results, for frequencies 5, 6 and 7 but for 3, 4 and 8 frequencies they are the same. When the number of frequencies is reduced (3 frequencies allocated to 40 links), most of the link orderings generated by the GA will not satisfy the interference constraint leading to a reduced search space. At the other extreme, the availability of 8 frequencies provides a higher degree of freedom for the GA such that many possible link orderings can give the optimal results within a small convergence time. The string that yields the best fitness in the current population keeps propagating successive generations and hence results in faster convergence. With an initial population size of 100 and a random generator for link orderings, the optimal results were obtained in less than 100 iterations for the above cases. But for the 5, 6 and 7 frequency cases the results were obtained after 5000 iterations.

The results for a 6×6 mesh are shown in Figure 4.11. The convergence of GA for 54 Mbps is better than that of the 11 Mbps case. In the latter case the SIR threshold is low and therefore many link orderings can satisfy the interference constraints, and hence a larger search space requires more iterations for convergence.

In Figures 4.12 and 4.13 comparisons between the mesh size and the number of frequencies are presented. It can be seen that the number of FSO links required for a 54 Mbps link is higher than an 11 Mbps link, which is again higher than a 1 Mbps link. This is expected since a higher SNR needs to be maintained for higher data

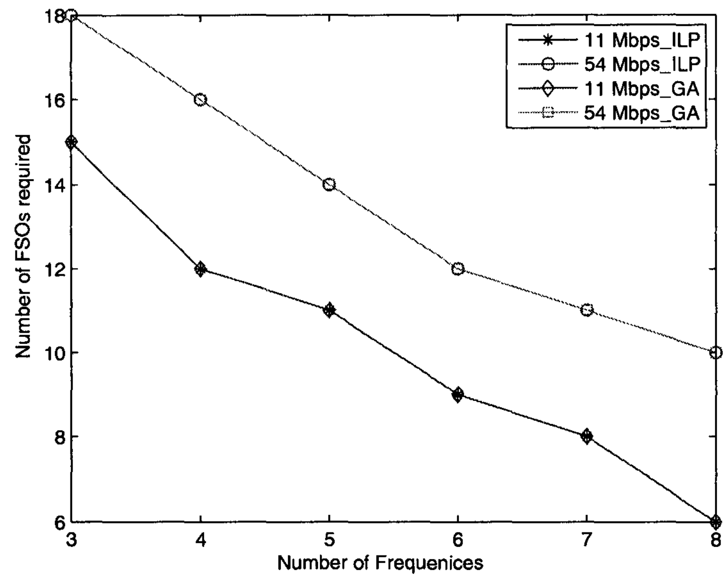

Figure 4.9: Integer programming and genetic algorithm results for 4×4 mesh with varying number of frequencies

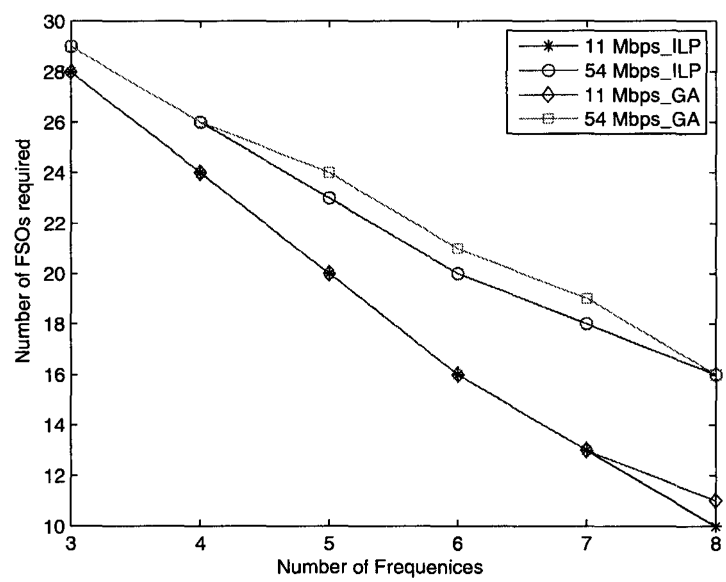

Figure 4.10: Integer programming and genetic algorithm results for 5×5 mesh with varying number of frequencies

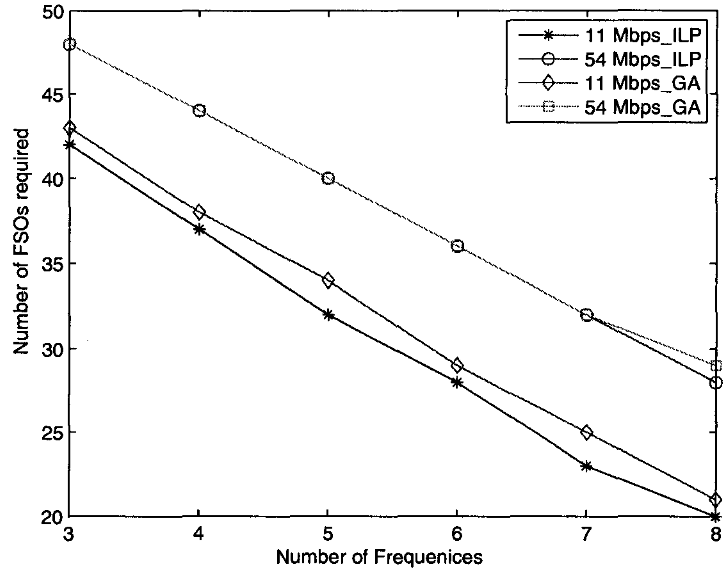

Figure 4.11: Integer programming and genetic algorithm results for 6×6 mesh with varying number of frequencies

rates and hence more FSO links are required. For a 3 frequency case, it is observed that the percentage difference in the number of required FSO links is very small for 1 Mbps and 54 Mbps. But for the 8 frequency case, as the mesh size increases above 7×7, there is a noticeable difference of 100% increase between 1 Mbps and 54 Mbps, and 65% increase between 11 Mbps and 54 Mbps in the number of FSO links required.

When the allocation is performed using 8 frequencies, there is more freedom to allocate channels in the center, but in this case the interference threshold between 11 Mbps and 54 Mbps becomes an important factor. The links in the center interfere with many others and the number of FSO links become highly sensitive to these thresholds. This is the reason for the noticeable difference as the mesh sizes increase above 7. For a 3 frequency case the degree of freedom is reduced and the interference threshold between 11 Mbps and 54 Mbps does not have much impact when allocating frequencies in the center of the mesh.

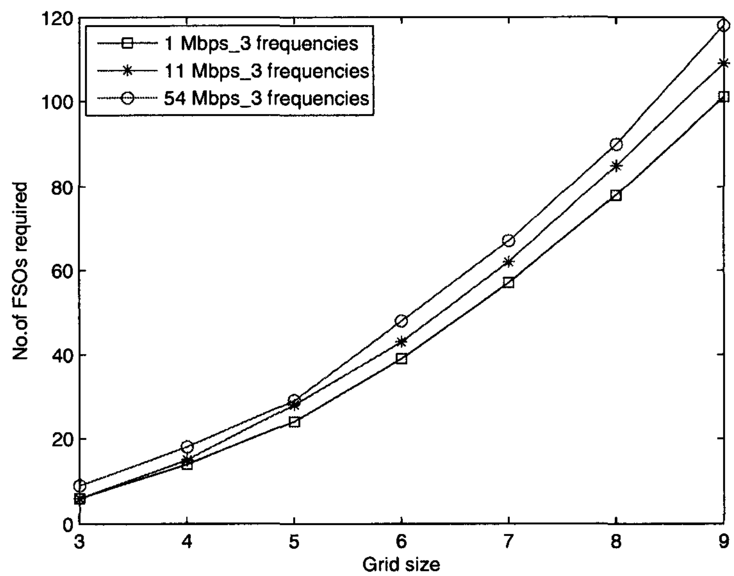

Figure 4.12: Genetic algorithm results for varying mesh sizes with 3 frequencies

In the next two results presented in Figures 4.14 and 4.15 the data rate is held constant and the influence on the number of frequencies is shown. There is a gradual decrease in the slope of the number of FSO links for a given mesh size as the number of frequencies vary. There is a more pronounced change in slope for higher mesh sizes, particularly 7×7 and 8×8. This is because of the increase in the number of links and with each successive increase in mesh size the number of interfering links also increases, causing more FSO links to be placed in the center.

The final two results in Figures 4.16 and 4.17 give the percentage of FSO links for different frequencies and for different data rates. Higher mesh sizes greater than 7×7 have higher numbers of FSO links particularly for 3 and 4 frequencies, where

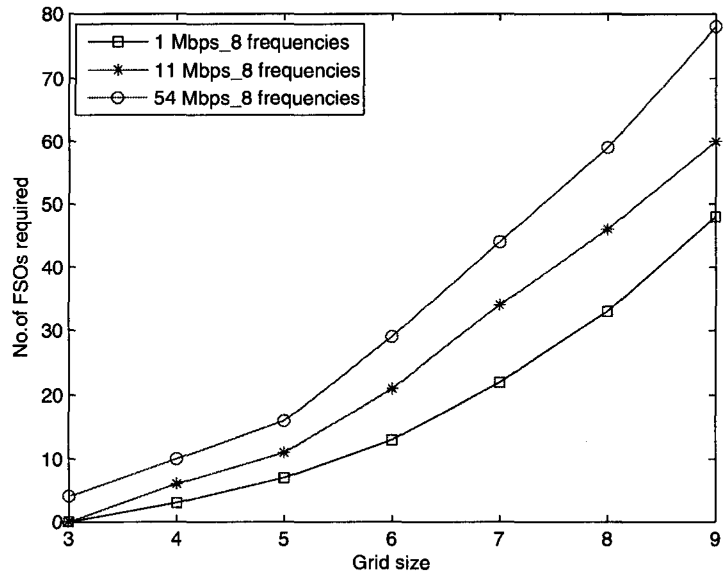

Figure 4.13: Genetic algorithm results for varying mesh sizes with 8 frequencies

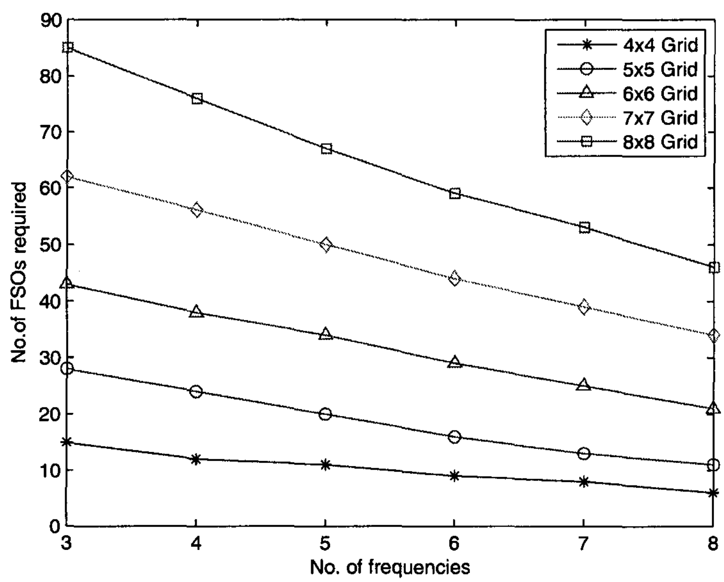

Figure 4.14: Genetic algorithm results for varying mesh sizes and frequencies for a data rate of 11 Mbps

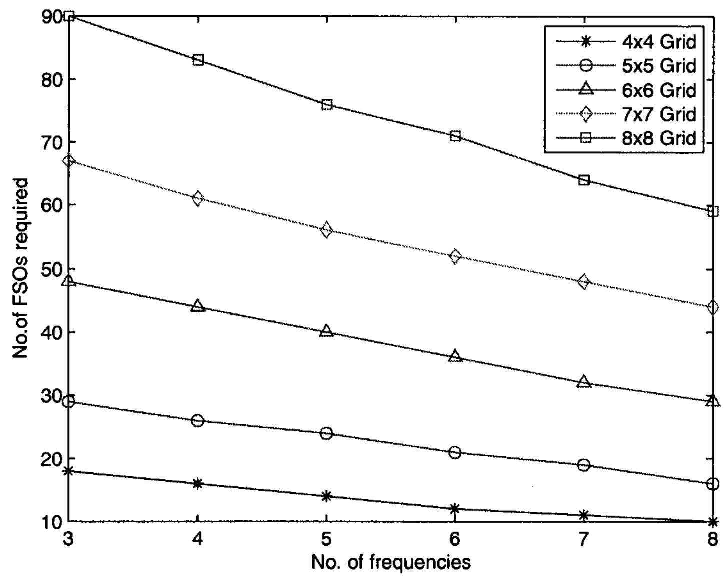

Figure 4.15: Genetic algorithm results for varying mesh sizes and frequencies for a data rate of 54 Mbps

more than 75% of the links in the mesh are FSO links and at least 50% of the links when the number of frequencies exceeds 5. For mesh sizes 3, 4 and 5, the percentage of FSO links in the grid are less than 35%. As the number of links in the center are very few for small grid sizes, only a few FSO links are required.

4.7.2 Frequency Assignment for Grid Structures with External Interference

When assigning frequencies to a newly deployed network there may be very little external interference. The interference between all of the links in the grid is calculated using a Piecewise Linear Exponential Path-Loss model. While trying to assign a particular frequency to a link, the interference criteria may not be satisfied. So the

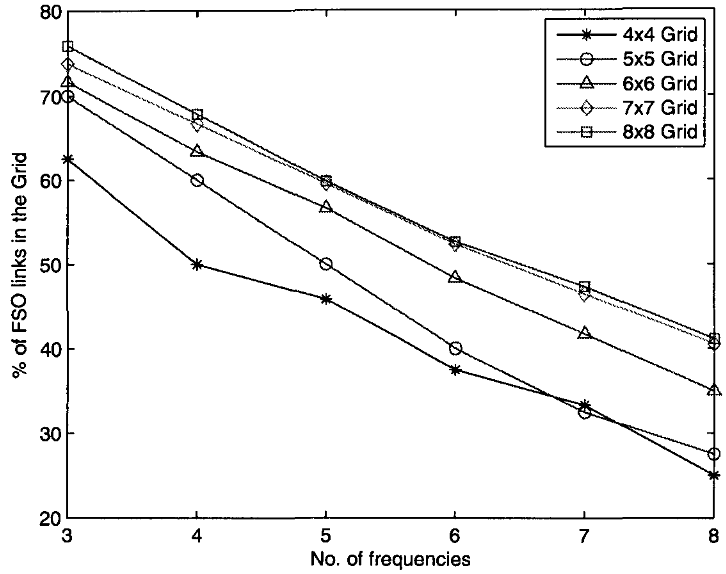

Figure 4.16: Percentage of FSO links in a grid for varying mesh sizes and frequencies for a data rate of 11 Mbps

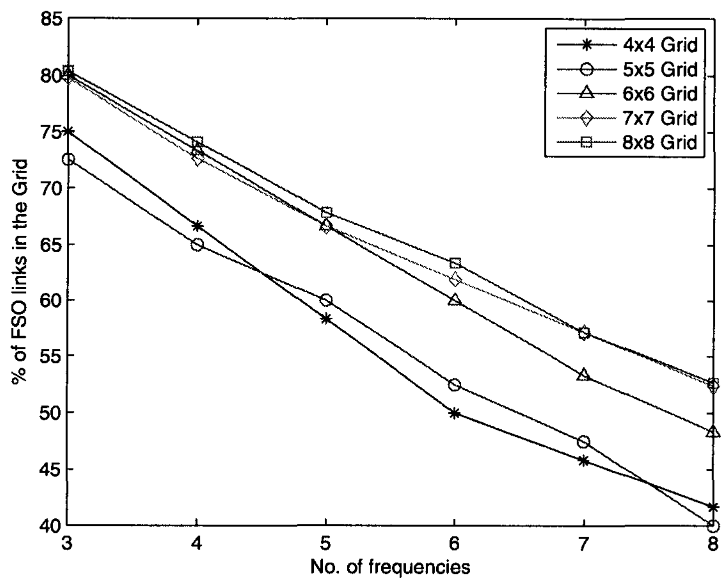

Figure 4.17: Percentage of FSO links in a grid for varying mesh sizes and frequencies for a data rate of 54 Mbps

frequency of either the interfering link or the interfered link can be changed and the frequency assignment can be tried again, as both are assignment frequencies. But in practical scenarios, there will always be some form of interference, like overlapping frequencies from other networks, broadband interference of which there is no control. An assignment has to be performed subject to this external co-channel interference. The ILP formulation in Equation 4.3 can be changed to include the co-channel interference from external APs as well, i.e.,

$$\forall i \in N', f \in K, \quad \sum_{j \in N': j \neq i} c_{ij} X_{jf} + I_{if} \leq B X_{if} + (1 - X_{if}) M \tag{4.7}$$

The term I_{if} denotes the interference received in link i for a frequency f from external interference. If the frequency f is to be allocated to a link, then the link i has to satisfy the interference received from all the co-channel interferers and external APs. In real-life scenarios, one has to measure the signal strength received for all of the overlapping frequencies in each of the link positions, and this information is fed as input to the algorithm. Thus, both the ILP and GA can be used to perform a frequency assignment in the presence of external APs with slight modifications to the interference constraints as explained in Equation 4.7.

The results for a 4×4 grid are shown in Figure 4.18. Frequency assignment has been performed with 8 frequencies, with each of the links operating at an 11 Mbps data rate. The external APs are distributed throughout the grid in a random fashion. FSO links are placed towards the center of the grid, as was observed in the results from the previous section.

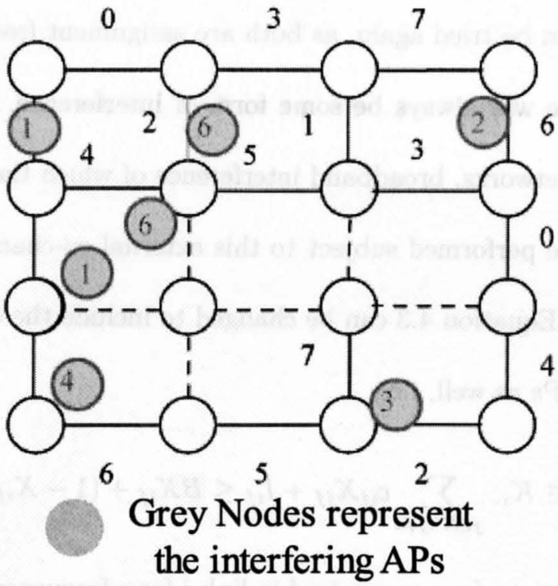

Figure 4.18: Frequency assignment results for 4×4 grid with external interfering APs

In the simulation performed for a 5×5 grid, shown in Figure 4.18, there is a concentrated external AP placement in the top-left-hand corner of the grid. Frequencies 0 and 1 are used by the external APs, essentially exhausting two frequencies from being assigned to the top-left region. Most of the links towards the edges have other non-overlapping frequencies assigned while FSO links are used towards the center of the grid.

4.7.3 Frequency Assignment for Non-Grid Structures

One of the major advantages of the proposed heuristic method is that it is not restricted to square mesh structures and can be used to solve any arbitrary placement of APs. The algorithm requires only the position of the APs, which are used to calculate the path loss between them. In this section, a McMaster University building layout

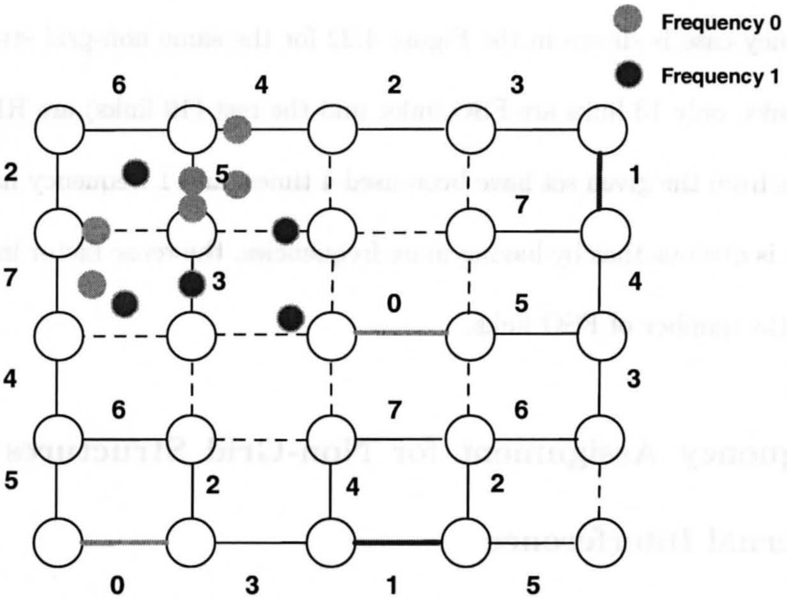

Figure 4.19: Frequency assignment results for 5×5 grid with two external frequencies overlapping in the top left region of grid

is used for AP placement, as it helps model practical scenarios. The APs are placed on a McMaster University building layout as in Figure 4.20. The network topology (links) is automatically calculated based on the distance of separation between the APs. There are 24 APs in the map, and the number of links calculated based on path loss is thirty-two.

The frequency assignment for these 32 links is performed with GA. Three colors, red, blue, and yellow denote the RF frequencies for the 3-frequency example, as shown in Figure 4.21. The green lines denote those links that are assigned as FSO links. Similarly, for the 5-frequency case, red, yellow, blue, brown, and violet have been used to denote RF frequencies, as in Figure 4.22. Again, green is used to denote an FSO link. From Figure 4.21, it is clear that out of 32 links, 19 are FSO links, and 12 are

RF links. Each of the 3 frequencies has been used 4 times (reuse factor). The result for the 5-frequency case is shown in the Figure 4.22 for the same non-grid structure. Out of the 32 links, only 13 links are FSO links, and the rest (19 links) are RF links. Four frequencies from the given set have been used 4 times, and 1 frequency has been used 3 times. It is obvious that by having more frequencies, the reuse factor increases and minimizes the number of FSO links.

4.7.4 Frequency Assignment for Non-Grid Structures with External Interference

The results for the non-grid structure can be extended to perform frequency assignment in the presence of external APs. Consider the case of a parallel wireless network operating inside McMaster University. Now a frequency assignment can be performed taking this external interference into consideration. Figure 4.23 shows the external APs, which are overlapping with the others. Three colors, yellow, blue, and red constitute the overlapping frequency spectrum. The external interference from these APs is given as input to the GA, and the frequency assignment is performed for a 3-frequency case and a 5-frequency case. In the 3-frequency example there is a complete overlap of the frequencies that need to be allocated and those of the external interfering APs. From Figure 4.24, it is observed that 22 out of 32 links are FSO links. The RF frequency reuse factor has been reduced because of the overlapping frequencies. In the area where there is the dense concentration of external APs, all the links are FSO. Here, also, green is used to denote an FSO link. In the 5-frequency example

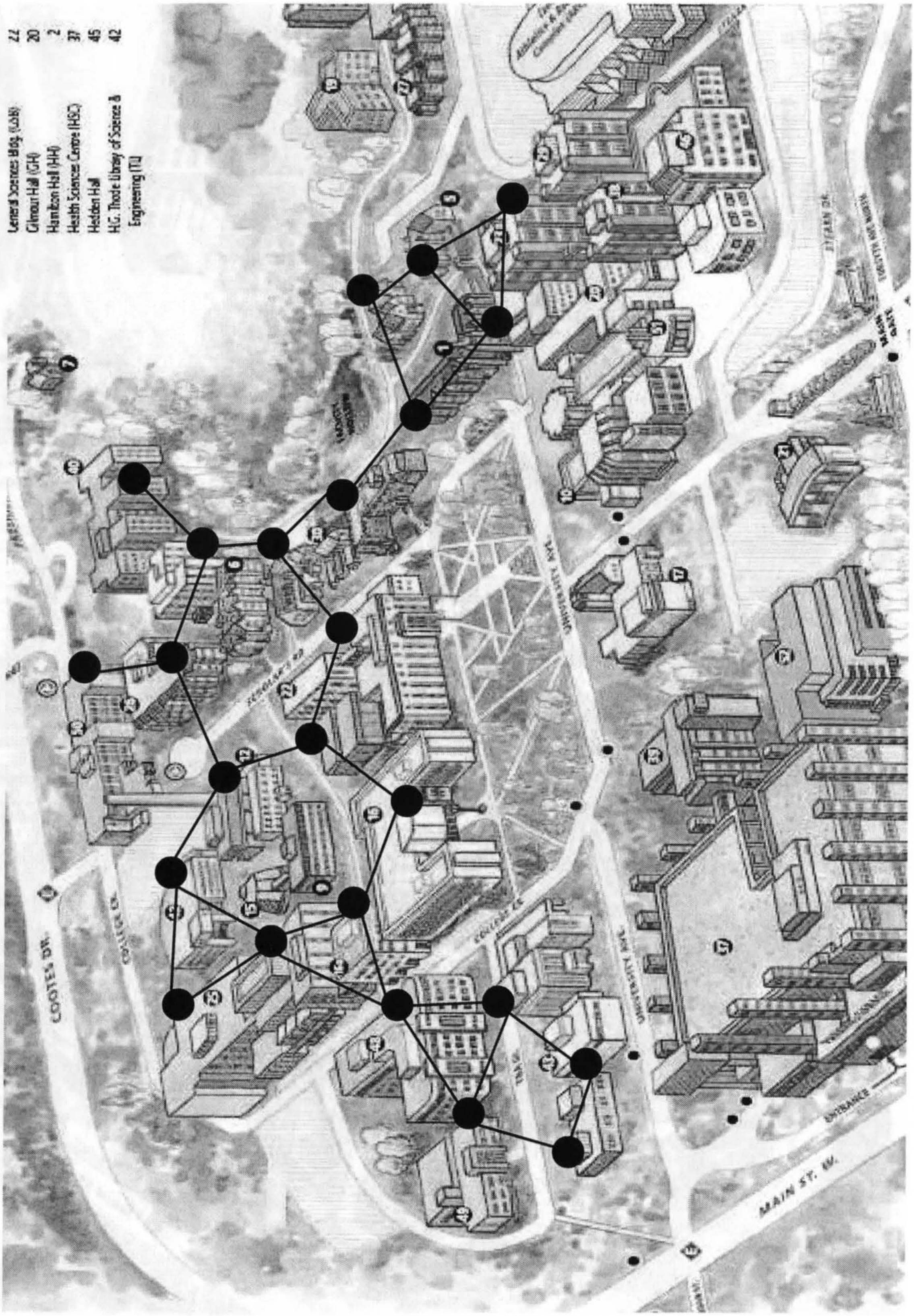

Figure 4.20: Non-grid structure AP placement (No. of APs=24, No. of links = 32)

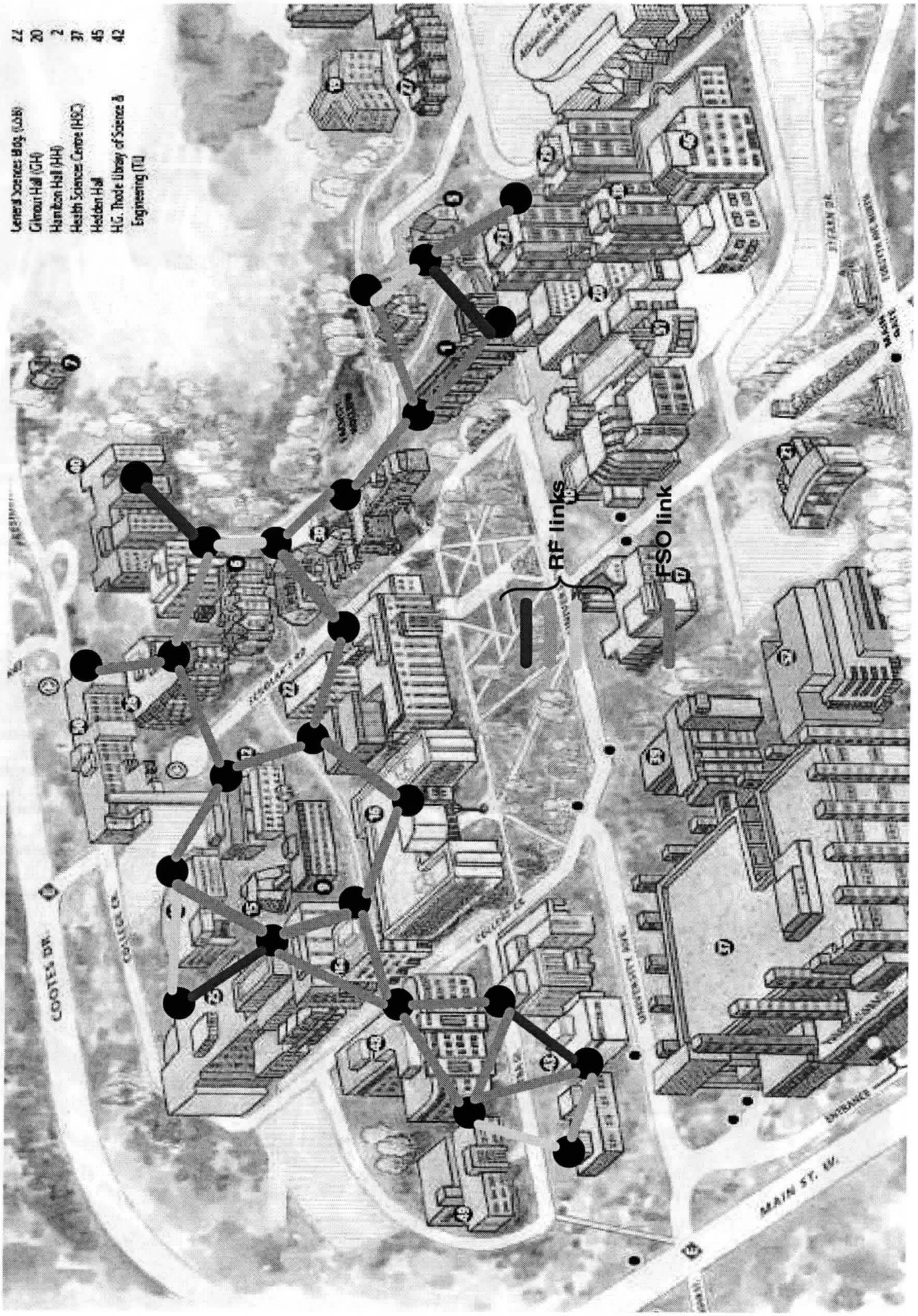

Figure 4.21: Frequency assignment result for the non-grid structure with 3 frequencies (No. of FSO links=19, No. of RF links=12)

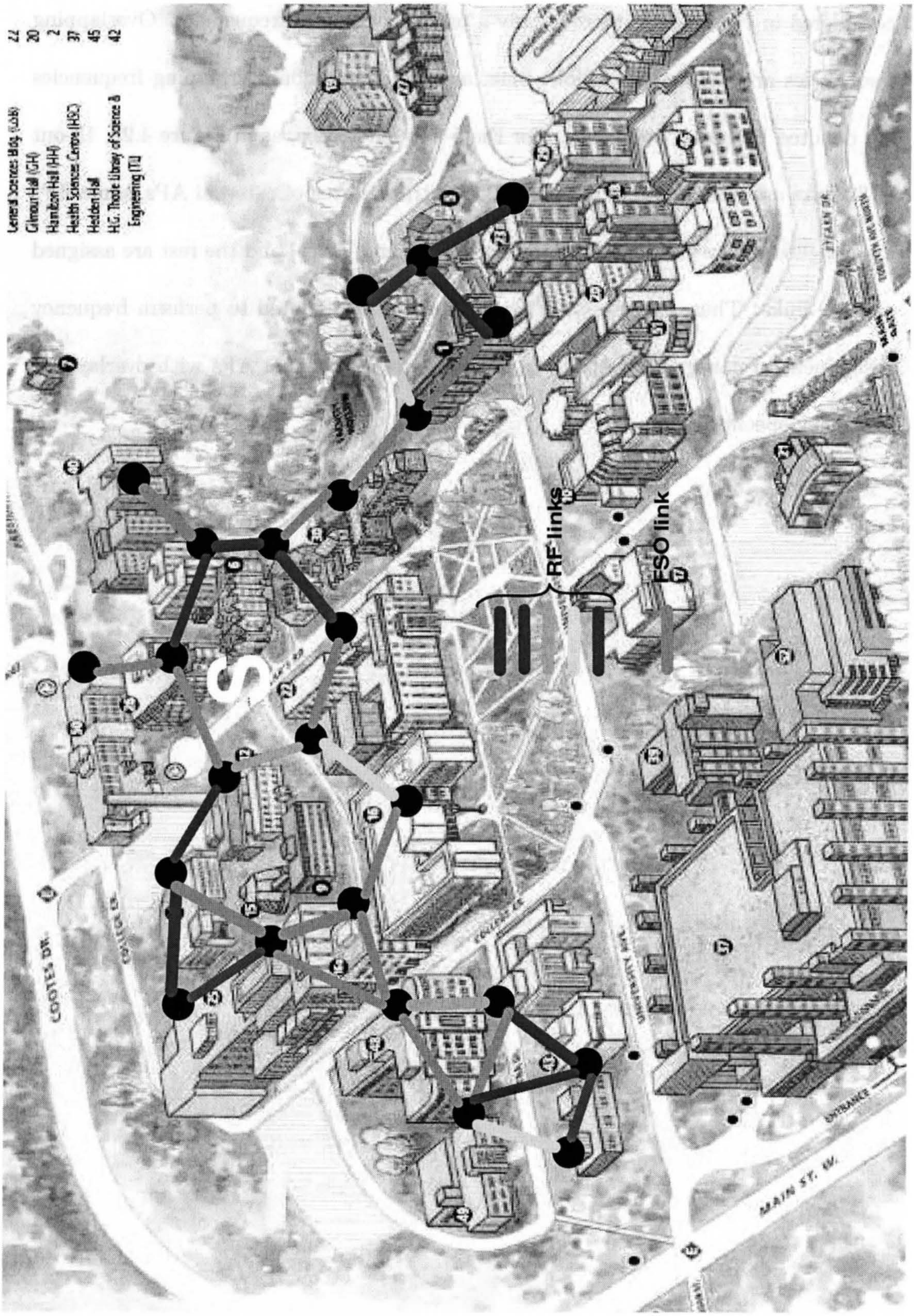

Figure 4.22: Frequency assignment result for the non-grid structure with 5 frequencies (No. of FSO links=13, No. of RF links=19)

considered in Figure 4.25, there is only a partial overlap of frequencies. Overlapping frequencies are denoted by yellow, blue, and red, while non-overlapping frequencies are denoted by brown and violet. For the 5-frequency case, as in Figure 4.25, 15 out of 32 links are FSO links. In the dense concentration area of external APs, some APs are assigned non-overlapping frequencies (brown and violet) and the rest are assigned as FSO links. Thus, the proposed algorithms can be adapted to perform frequency assignment of non-grid structures in the presence of external APs with overlapping frequency specifications.

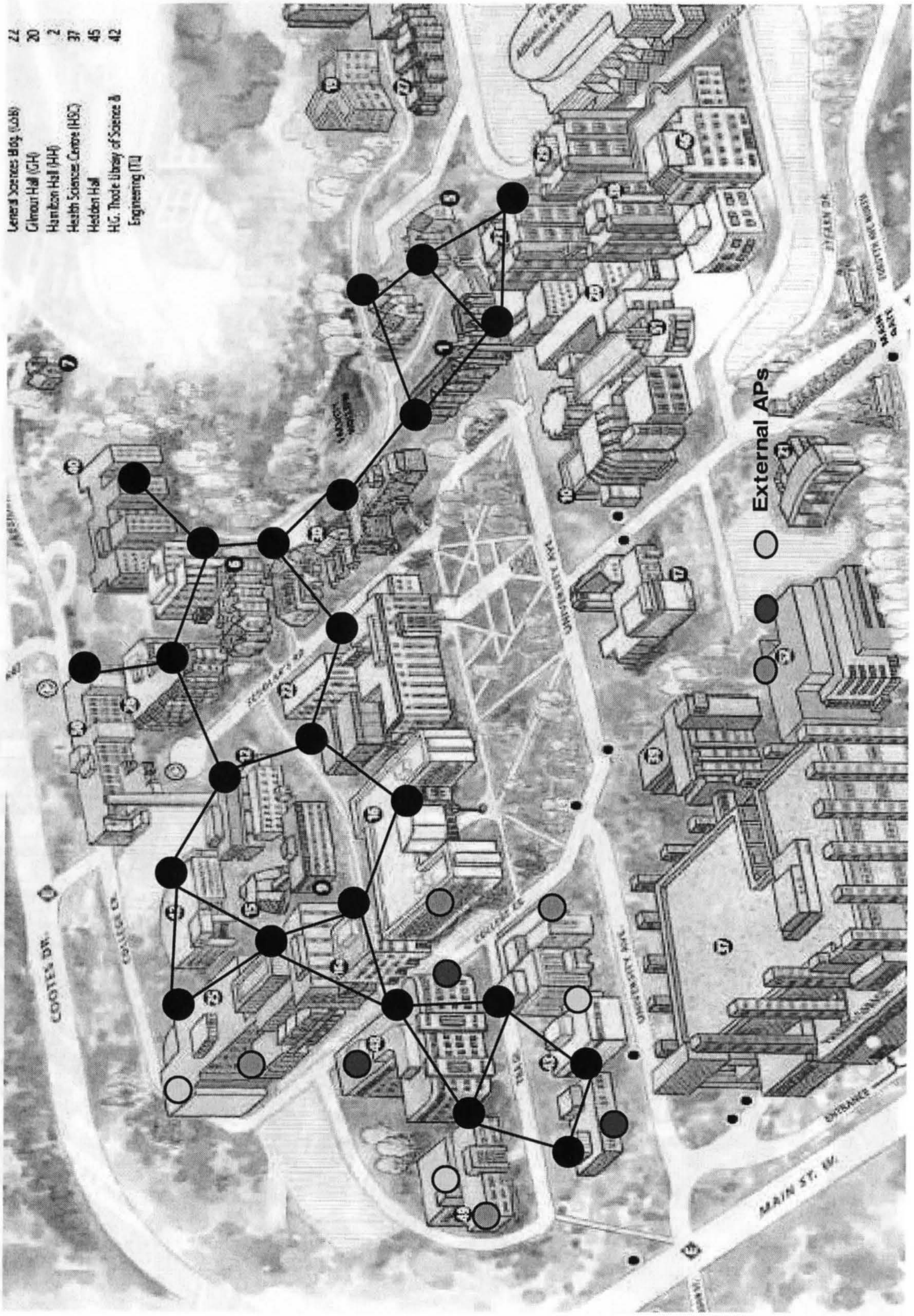

Figure 4.23: Non-grid structure AP placement with interfering APs

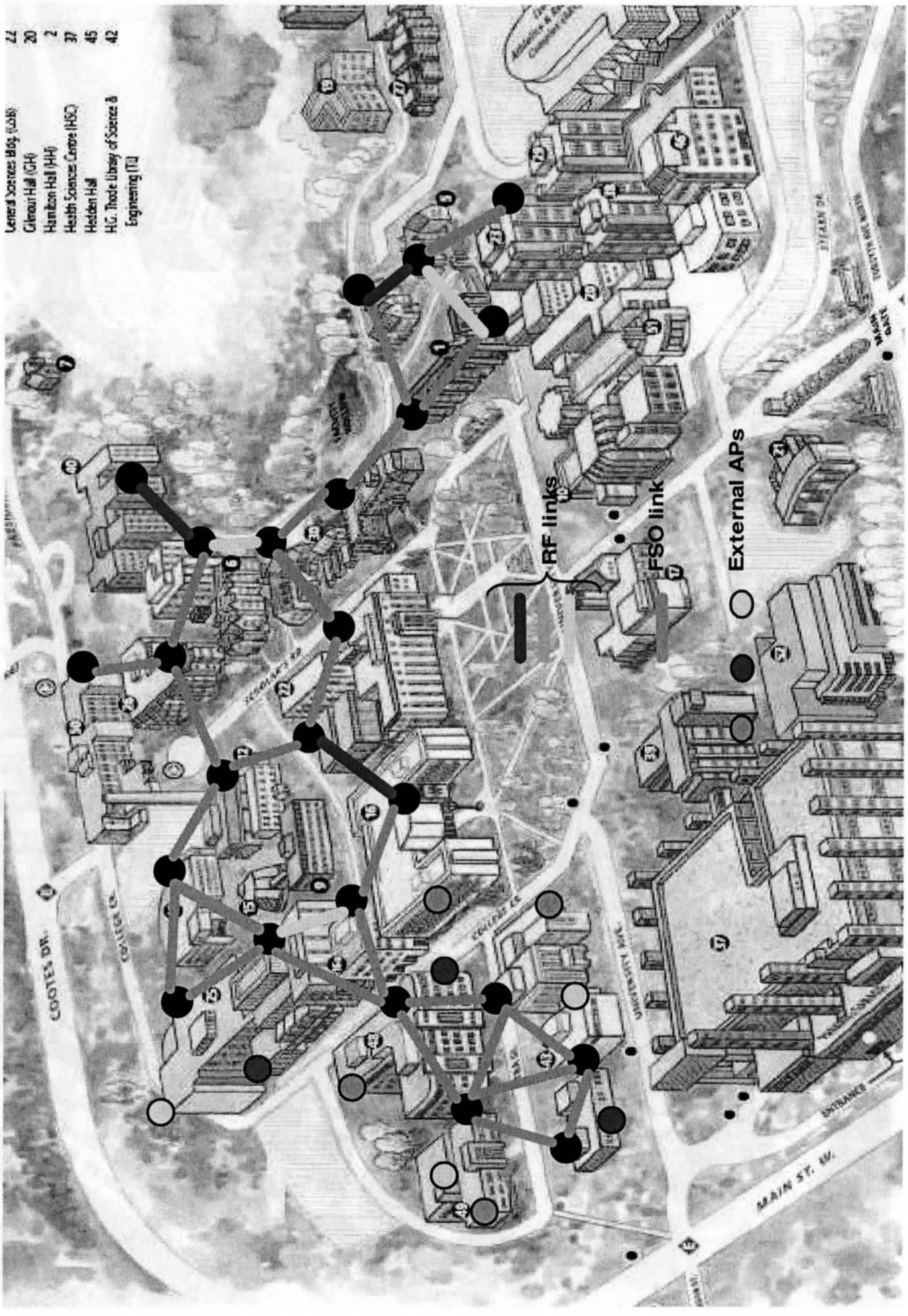

Figure 4.24: Frequency assignment result for the non-grid structure with 3 frequencies and external interfering APs (No. of FSO links = 22, No. of RF links = 10)

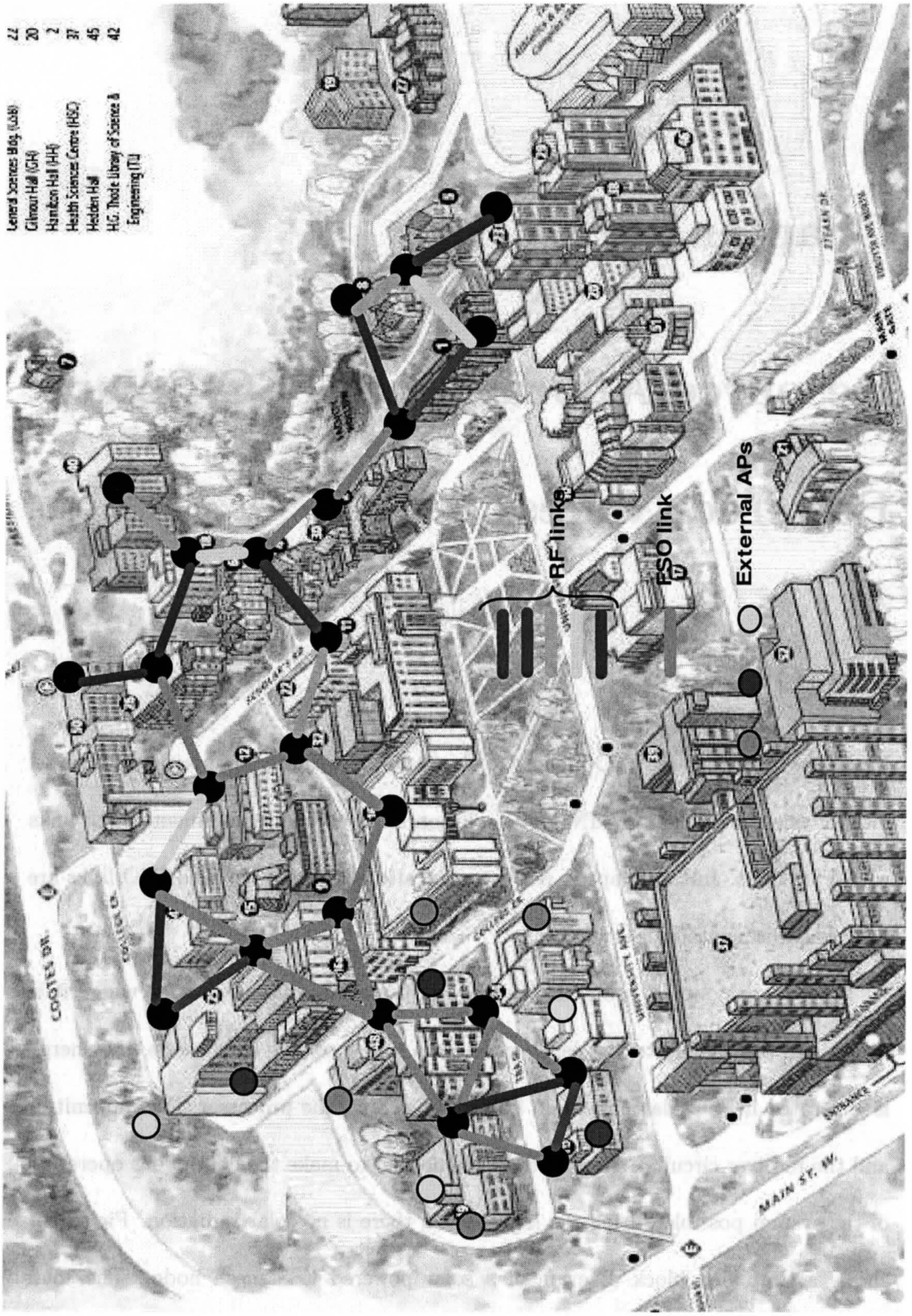

Figure 4.25: Frequency assignment result for the non-grid structure with 5 frequencies and external interfering APs (No. of FSO links = 15, No. of RF links = 17)

Chapter 5

Resource Allocation of FSO Solar Powered Nodes

5.1 Overview

In the previous chapter, FSO links were shown to be useful in eliminating co-channel interference prevalent in WMNs. The solution required the replacement of RF links with FSO links. In this chapter, resource allocation for these replaced FSO links are performed using statistical methods.

WMNs are powered using solar energy in certain outdoor scenarios where it is difficult to provide electricity using wires. In a solar powered mesh node, the energy is generated in the solar panel and it is consumed by the processor, the transmitter and the receiver circuits. Also, a battery is needed to make the continuous operation of the system possible during the night, when there is no solar radiation. Figure 5.1 shows a simplified block diagram of a solar powered ESS mesh node. The solar panel and the battery are connected to the AP through a charge controller, which prevents battery over and under charge. The solar panel and battery (resources) form a significant fraction of the overall node provisioning cost. While resources have been allocated to all existing RF links in a WMN, resource allocation for the newly assigned FSO links also needs to be performed. Resource estimation for FSO links is very important as it helps us to determine whether any extra resources are required. FSO links consume less power than RF links, as seen in Chapter 3, and as a result the overall power consumption of the node can be reduced. Therefore the amount of resources required can be reduced and as a result the overall cost of the node can also be minimized. For this reason, resource allocation must be done accurately to obtain a minimum cost solution, which also guarantees some desired performance levels.

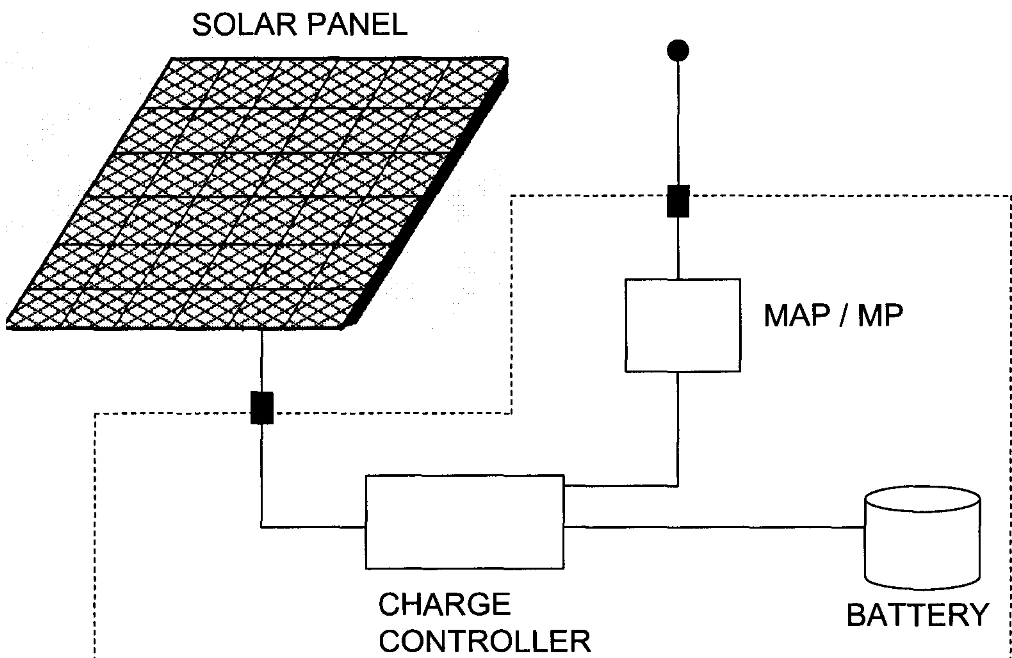

Figure 5.1: A solar powered access point model

In the rest of this chapter the structure of the energy flow model and simulation method proposed in [29] are explained. A simple methodology for calculating the power requirements of FSO links and RF links has been proposed. Based on these power estimates, panel and battery sizes are calculated using statistical methods. From the contour curves of panel and battery sizes for two different cities, namely, Phoenix and Toronto, the panel and battery size that results in the minimum cost are derived. The minimum cost resource allocation results for different node configurations and throughputs are also presented in the results section.

5.2 Background

The resource allocation procedure in a solar powered mesh node determines the actual battery and panel size required to support the node. The solar panel and battery size depend on two other stochastic parameters, namely the load on the AP and the amount of the incident solar radiation. Since there is no deterministic model for these stochastic parameters, the statistical resource allocation method proposed in [29] is used for resource allocation. In a statistical method, the measure of success or failure is also probabilistic. Therefore, the system performance can be represented by the statistical term called P_{out}, which is

$$P_{out} = \frac{No.\ of\ hours\ lost\ due\ to\ power\ outage}{Total\ no.\ of\ hours\ in\ a\ year} \tag{5.1}$$

Provisioning of the solar panel and the battery is largely dependent upon the value of P_{out} and is generally performed to guarantee a given P_{out}. The charging of the battery depends on the amount of solar insolation data and is obtained from the publicly available meteorological data. The statistical method used in this thesis primarily relies on the assumption that the weather pattern is cyclo-stationary and a sufficiently large analysis of the historical weather data in calculating the resources will lead to a fairly reliable estimate for the future. The following section presents details about the energy flow model used in the statistical method.

5.2.1 Energy Flow Model

The energy flow model proposed in [29] defines different terms relating to the formulation of the energy balance equation in solar powered APs. The energy flow model is based on two events: One is the charging event due to the solar power and the other event is the power consumption of the transmitter and the receiver.

Some of the terms used in the energy flow model are as follows. $\varepsilon_{panel}(k)$ is the energy produced in the solar panel over the time increment [(k- 1) Δ, kΔ], and Δ is the time-step length considered (1-hour increments). $B(k)$ is the residual battery energy stored at a time kΔ, and B_{max} is the maximum battery capacity. B_{outage} is the maximum allowed depth of battery discharge. $L(k)$ is the load energy demand over the time duration, [(k- 1) Δ; kΔ]. The energy flow can be stated as follows,

$$B(k) = min\left\{max\left[B(k-1) + \varepsilon_{panel}(k) - L(k), B_{outage}\right], B_{max}\right\}, \qquad (5.2)$$

where $B(k)$ is the residual battery energy stored at time kΔ and it is bounded between B_{outage} and B_{max}. Load ($L(k)$) on the SMAP is dependent on the data rate and throughput the link. If the throughput is the same as the data rate, then the power consumption is equal to the power consumption of either the FSO link or the RF radio. However, if the operating throughput is different from that of the data rate, then the link needs to be operational only for the fraction of time required to achieve the desired throughput. The radio can be in power-save mode during the rest of the time. A detailed discussion regarding different power saving techniques is presented in [32].

5.3 Power Consumption Estimates for RF and FSO Nodes

In this section, the power consumption values of an FSO link and an RF link are analyzed for different throughputs. The data rate of the FSO link is 155 Mbps, as referred to in Chapter 3. FSO transmitters and receivers are connected to the host processor with an Ethernet interface. A fixed power consumption of 1 W is added to the estimates obtained as the power consumed in the host processor. The actual overhead in an FSO link is the overhead due to the Ethernet interface. The Ethernet interface can carry a maximum packet size of 1500 bytes and the packet size used in the simulations is 2000 bytes. The overhead in an Ethernet MAC frame consists of Inter-frame spacing, preamble, MAC header, trailer, network and transport layer headers and their overall sum is given in the following equation,

$$FSO_{over} = 78\ bytes. \tag{5.3}$$

Let $P_{size} = 2000$ denote the packet size, and $E_{size} = 1500$ denote the maximum packet size that can be carried by an Ethernet frame. Let $P_{fso\_tx} = 80mW$ and

$P_{fso\_rx} = 60mW$ be the transmit and receive powers for the FSO link. Let Th_{rate_fso} denote the throughput to be maintained in the link and D_{rate_fso} denote the data rate of the link.

An FSO link operates at 155 Mbps and it replaces an RF link operating at a much lesser throughput. Therefore, an FSO link need to be operational only for a certain period of time and the time required (T_{ref_time}) for the link to be active is the fraction of the time required to achieve the required throughput (Th_{rate_fso}). This is calculated in the following equation as,

$$T_{ref\_time} = \frac{Th_{rate\_fso}}{D_{rate\_fso}} . \tag{5.4}$$

The amount of time required to keep an FSO link in an ON state for transmission and reception is dependent upon the packet size. As the actual packet size used in the simulation is higher than the maximum packet size that can be carried by an Ethernet link, it has to be split and sent as two packets. The total number of packets (N_{fso}) and the time required (T_s) to transmit a packet of 2000 bytes are shown in the following equations,

$$N_{fso} = \lceil \frac{P_{size}}{E_{size}} \rceil , \tag{5.5}$$

$$T_s = \frac{(N_{fso} - 1)(FSO_{over} + E_{size}) + FSO_{over} + P_{size} - ((N_{fso} - 1)E_{size})}{D_{rate\_fso}} . \tag{5.6}$$

As FSO links are full duplex, the transmitter and the receiver circuits are ON at the same time. The total power consumption per packet P_s is the sum of transmitter (P_{fso_tx}) and receiver power (P_{fso_rx}) consumptions. From the time required to transmit one packet in Equation 5.6, the power required to transmit a packet is calculated in the following equation as,

$$P_s = T_s P_{fso\_tx} + T_s P_{fso\_rx} \ . \tag{5.7}$$

The total power consumption required to achieve the given throughput is calculated as the total number of packets to be transmitted multiplied by the power consumption for a single packet, which is given in the next equation as,

$$P_{thru} = \frac{T_{ref\_time}}{T_{single}} P_s \ . \tag{5.8}$$

Thus, the power consumption value of an FSO link (transmitter and receiver) is obtained and a constant power of 1W is added to this estimate as the power required by the host processor. Similarly, the power consumption of an RF link also can be performed. For an RF link, the overhead bytes are transmitted at different rates. RF overhead which include the PLCP preamble, the PLCP header and the ACK overhead are transmitted at 1 Mbps. Other overhead bytes due to the MAC header (70 bytes) are transmitted at 54 Mbps along with the data. Let Th_{rate_rf} denote the throughput to be maintained in the link and D_{rate_rf} denote the data rate of the RF link, which is 54 Mbps. Let $E_{size} = 2264$ denote the maximum packet size that can be carried by an IEEE 802.11 MAC frame. Let $P_{rf\_tx} = 780mW$ and $P_{rf\_rx} = 480mW$ be the transmit and receive powers of the RF transmitter and receiver respectively. The overhead calculations in an RF link are shown in the equations below,

$$RF_{over} = 24 \ bytes \ , \tag{5.9}$$

$$ACK_{over} = 14 \ bytes. \tag{5.10}$$

The overhead in Equations 5.9 and 5.10 are transmitted at 1 Mbps, whereas the MAC overhead (M_{over}) shown in the following equation, is transmitted at 54 Mbps.

$$M_{over} = 70 \; bytes. \tag{5.11}$$

The total number of packets (N_{RF}) and the time required (T_s) to transmit a packet size of 2000 bytes are shown in the next set of equations,

$$T_{ref\_time} = \frac{Th_{rate\_rf}}{D_{rate\_rf}} , \tag{5.12}$$

$$N_{RF} = \lceil \frac{P_{size}}{E_{size}} \rceil , \tag{5.13}$$

and

$$T_s = 8 \left[\frac{RF_{over} + ACK_{over}}{1Mbps} \right] \left[(N_{RF} - 1) \frac{M_{over} + E_{size}}{D_{rate\_rf}} + \frac{M_{over} + P_{size} - (N_{RF} - 1)E_{size}}{D_{rate\_rf}} \right] . \tag{5.14}$$

An RF radio operates in half-duplex mode and so the total power consumption of a packet P_s is the average of transmitter (P_{rf_tx}) and receiver power (P_{rf_rx}) consumptions. The transmitter is ON approximately half of time and the receiver is ON for the rest of the time. From the time required to transmit one packet in Equation 5.14, the power required to transmit a packet is calculated in the following equation as,

$$P_s = T_s \frac{P_{rf\_tx} + P_{rf\_rx}}{2} . \tag{5.15}$$

The total power consumption required to achieve the given throughput is calculated as the total number of packets to be transmitted multiplied by the power consumption for a single packet, i.e.

$$P_{thru} = \frac{T_{ref\_time}}{T_{single}} P_s . \tag{5.16}$$

Figure 5.2 compares the power requirements for an FSO link with those of an RF link for different throughputs. It can be observed that FSO links consume less power

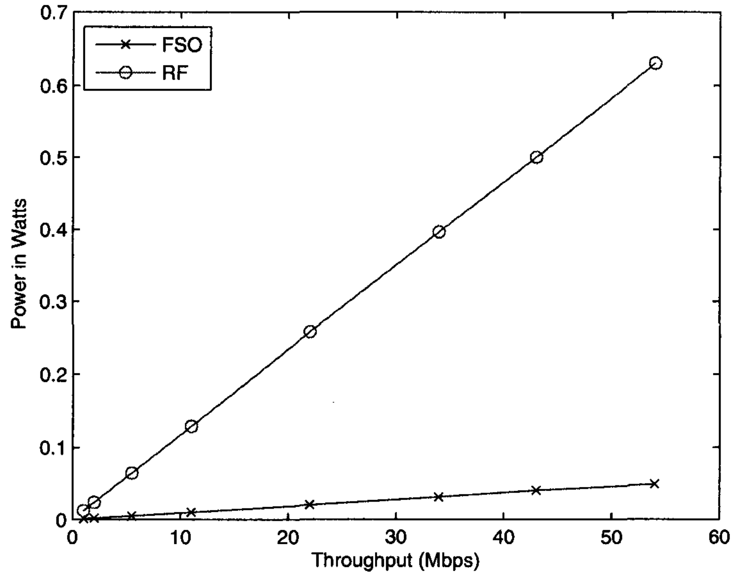

Figure 5.2: Power consumption values of FSO and RF links for different throughputs

compared to RF links at higher data rates. RF circuits consume more power per packet and as the throughput increases, more packets need to be transmitted. Hence, there is a significant change in the power consumption of RF links compared to FSO links at higher throughputs.

5.4 Simulation Method

The statistical approach provides the minimum cost of the battery and the panel size for provisioning a solar powered node which guarantees a desired outage probability. Different combinations of panel and battery size estimates are obtained for a given node (RF or FSO) by simulating it over the solar insolation data and power consumption values. Each combination of panel and battery size gives a different P_{out}

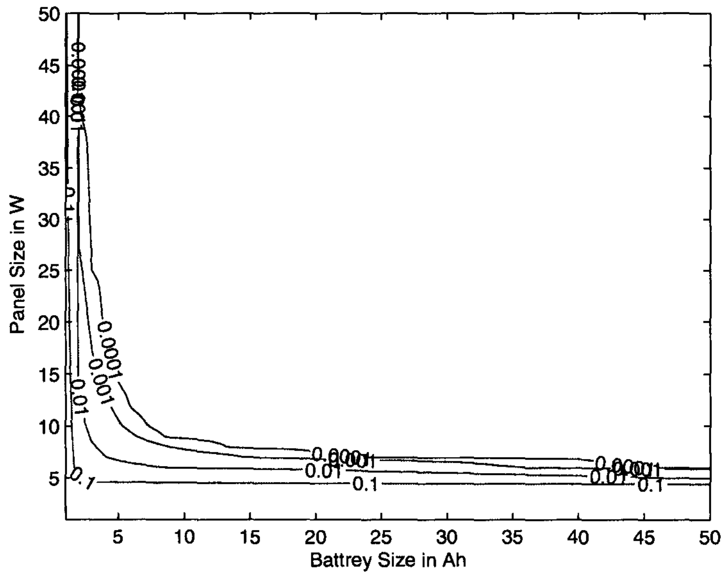

Figure 5.3: Contour plot for different outage probabilities (Phoenix)

and different combinations that give the same P_{out} are shown as contour curves in Figures 5.3 and 5.4. With the cost details of buying a solar panel and battery for per watt of power, the total cost of a node can be obtained and the solution that gives the minimum cost is the preferred one. The cost estimates for different outage probabilities and node configurations of RF nodes and FSO nodes are shown in the results for two different cities, namely Phoenix and Toronto. Phoenix receives ample sunlight and the outage events are less compared to a more moderate climatic region like Toronto where solar insolation is dependent on the particular time of the year.

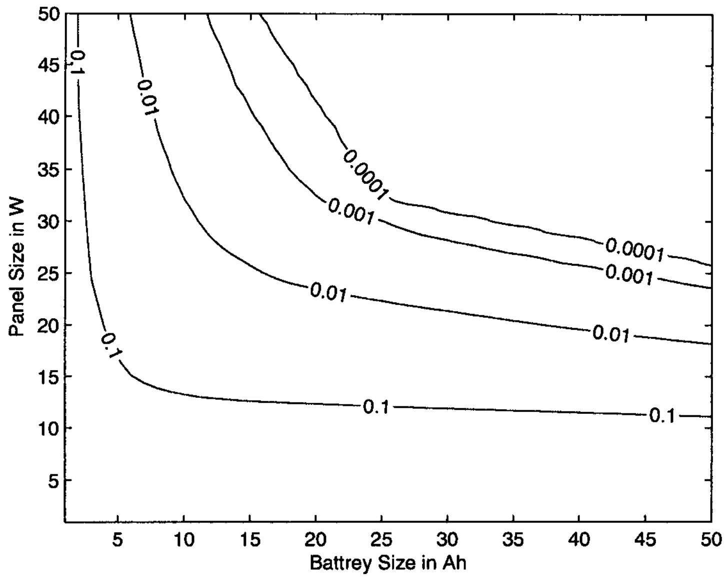

Figure 5.4: Contour plot for different outage probabilities (Toronto)

5.5 Results

In this section the comparison between the minimum cost resource allocation of RF and FSO nodes is presented. A mesh node has a minimum of two links (edges) and a maximum of four links (center) and it is assumed that all of them are operating simultaneously. In this chapter, power comparison results for the case of 4 links are provided and their minimum cost resource allocation results are compared. The maximum data rate of the RF link is 54 Mbps and throughputs are set at 1, 2, 5.5, 11, 22, 34, 48 and 54 Mbps. FSO links operate at 155 Mbps and hence needs to be operational only for the fraction of time required to achieve the desired throughput. Tables 5.1, 5.2, 5.3 show the minimum cost solution obtained for different node configurations and outage probabilities.

Table 5.1: Minimum cost resource allocation of FSO nodes for different throughputs and a P_{out} of 10^{-2} (Phoenix)

Phoenix			
Throughput	Battery Size	Panel Size	Cost
1	3.386	6	51.51
2	3.415	6	51.61
5.5	3.54	6	52.04
11	3.758	6	52.78
22	4.3	6	54.62
34	5	6.07	57.47
48	4	6.94	59.86
54	4.123	7	60.69

Table 5.2: Minimum cost resource allocation of RF nodes for different P_{out} values (Toronto)

Throughput	$P_{out} = 10^{-4}$	$P_{out} = 10^{-2}$	$P_{out} = 0$
1	194.11	142.12	197.8
2	203.47	148.32	207.85
5.5	232.46	170.45	238.04
11	279.64	205.16	284.98
22	374.35	274.36	378.86
34	482.55	350.26	489.72
48	590.98	438.05	601.2
54	644.62	480.89	656.34

Table 5.3: Minimum cost resource allocation of FSO nodes for different P_{out} values (Toronto)

Throughput	$P_{out} = 10^{-4}$	$P_{out} = 10^{-2}$	$P_{out} = 0$
1	185.75	136.02	187.73
2	186.27	136.65	191.10
5.5	189.01	138.42	191.13
11	193.64	141.16	197.8
22	200.35	146.36	204.46
34	207.55	152.26	211.26
48	216.98	159.05	221.33
54	221.62	161.89	224.6

The first comparison provided here is between the minimum cost resource allocation of FSO nodes and RF nodes for different P_{out}. At a maximum throughput of 54 Mbps for the Phoenix region, there is a cost difference of 200% for a P_{out} of 10^{-4} and 142% for a P_{out} of 10^{-2} between FSO and RF nodes, as observed in Figures 5.5 and 5.6. Similarly for the Toronto region, the cost difference is 300% for a P_{out} of 10^{-4} and 200% for a P_{out} of 10^{-2}, as shown in Figures 5.7 and 5.8. FSO links require much lesser resources compared to RF links and hence no extra provisioning is required when replacing RF links with FSO links.

The next comparison is based on the minimum cost resource allocation results for a given P_{out} at different throughputs. From the results in Table 5.1, it can be observed that there is only a marginal cost increase of 3.2% between an FSO link operating at 1 Mbps and 54 Mbps. On the contrary, for an RF link, there is a cost difference of about 59% when operating at 1 Mbps and 54 Mbps as seen in Figure 5.5. This clearly indicates that FSO links can provide a significant cost advantage at higher throughputs with a marginal increase in resource allocation costs. The method proposed in this thesis compares resource allocation cost results of FSO and RF links, but apart from that there are other factors like equipment costs, setup and installation costs which have not been taken into account.

From the above results, it can be observed that FSO links consume less power compared to RF links and thus, do not require any extra provisioning when interfered RF links are replaced with FSO links.

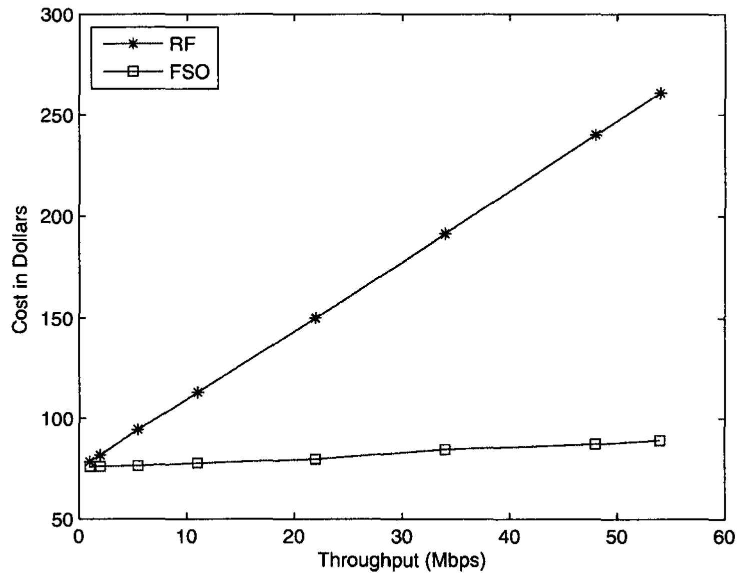

Figure 5.5: Minimum cost resource allocation results for different throughputs and a $P_{out} = 10^{-4}$ (Phoenix)

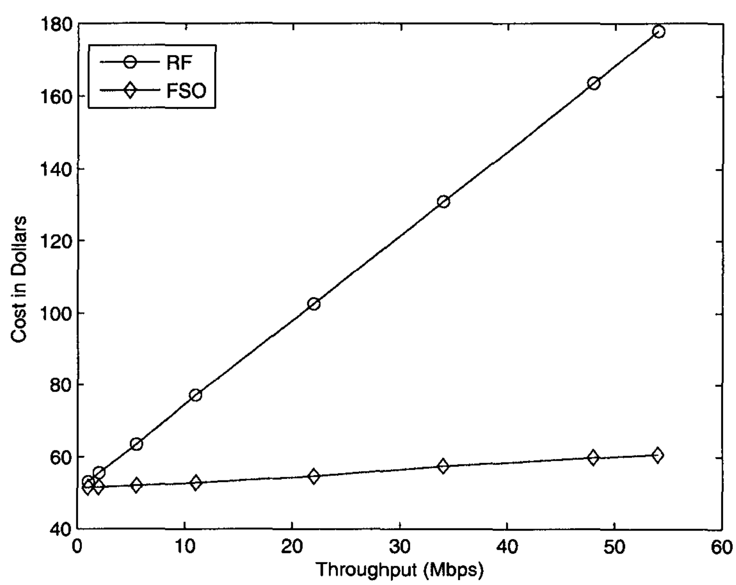

Figure 5.6: Minimum cost resource allocation results for different throughputs and a $P_{out} = 10^{-2}$ (Phoenix)

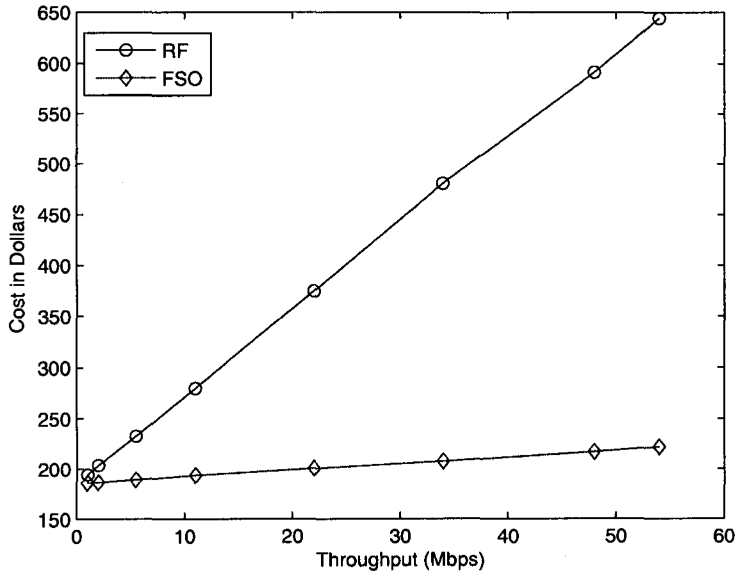

Figure 5.7: Minimum cost resource allocation results for different throughputs and a $P_{out} = 10^{-4}$ (Toronto)

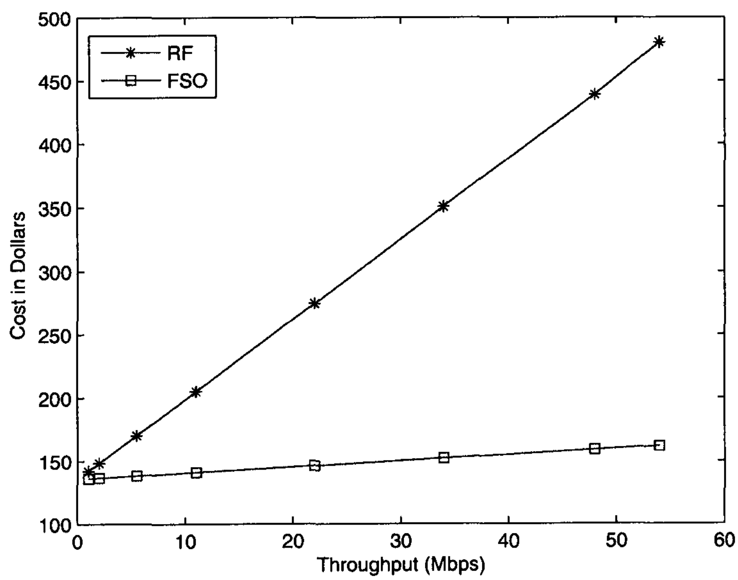

Figure 5.8: Minimum cost resource allocation results for different throughputs and a $P_{out} = 10^{-2}$ (Toronto)

Chapter 6

Conclusions

In this thesis the use of an FSO link as a replacement for an interfered RF link has been proposed. The FSO link-replacement problem was formulated as a graph coloring problem and the NP-completeness of the problem was proven. The problem was solved using an integer programming approach and a genetic algorithm. The results show that for small mesh sizes the genetic algorithm provides comparable results to that of the optimal values given by the integer programming formulation. The proposed frequency assignment solutions were also used for non-grid structures. FSO deployment scenarios was also extended in this thesis to mitigate the effect of external interference.

When replacing the interfered RF links in energy-sustainable solar power nodes, the resource utilization of these new FSO links was also considered. The power consumption of FSO links was compared to that of RF links based on their transmitter and receiver power consumption. It was found that significant reductions in resource allocation and node cost can be achieved using FSO links. The performance results for different node configurations and data rates were also presented. Thus, FSO links prove to be a viable solution in solving the interference problem in WMNs without any increase in node provisioning costs. In the future, there may be an integration of radio and optical technologies to a greater extent, combining the benefits of both the technologies. The work done in this thesis can be extended to solve the following problems.

1. Capacity Constraint

   FSO links were used as a replacement in interference-prone WLAN mesh networks. However, the capacity advantage obtained by replacing an RF link with an FSO link was not considered. An FSO link can theoretically provide atleast three times more bandwidth than that of an RF link. This increase in bandwidth can be utilized by running shortest path routing on these replaced links. In this way, the capacity of FSO links can be used to provide additional bandwidth to the network.

2. Delay-Bound and Routing Design

   A WLAN mesh network is usually deployed based on providing a certain end-end latency. In an interfered network, the end-end latency may be affected as a result of frequent collisions and retransmissions. An interesting formulation in an interfered network would be to find the minimum number of FSO links required to achieve the end-end latency for which the network was originally designed. The capacity advantage provided by the replaced FSO links can be used to route traffic to minimize the overall delay.

3. Dual Mesh Radio

In the future, the convergence of optical and wireless networks could be a possibility. FSO links can be operated as primary links and when link degradation occurs due to alignment errors or line-of-sight obstructions, RF links can be used as backup links. A mesh node in a grid structure will have 4 FSO links towards the center of the grid but a single RF radio can provide backup to all the FSO links. When an FSO link goes down, RF radios have to be triggered at both ends. One way to do the triggering is to send feedback regarding the bit error rate (BER) and the status of the FSO links periodically through the RF links. The time interval between successive feedback should not be too small, as frequent triggering of RF links consumes power. Optimum feedback interval calculation and a protocol for operating the dual mesh radio can be developed.

Bibliography

[1] HMIT Roofnet. http://www.pdos.lcs.mit.edu/roofnet/. Science and Artificial Intelligence Laboratory, MIT, Cambridge, MA.

[2] Seattle Wireless. http://www.seattlewireless.net/. Seattle, WA.

[3] Cisco Systems. http://www.cisco.com/. San Jose, CA.

[4] Southampton Open Wireless Network. http://www.sown.org.uk. Southampton, UK.

[5] T. S. Rappaport. *Wireless Communications, Principles and Practice.* Prentice Hall, 1996.

[6] J. F. Hayes. *Modeling and Analysis of Computer Communications Networks.* Plenum Press, 1986.

[7] IEEE Standards Department. *IEEE Draft Standard - Wireless LAN.* IEEE Press, 1996.

[8] B. S. Borowy and Z. M. Salameh. Optimum photovoltaic array size for a hybrid wind/PV system. *IEEE Transactions on Energy Conversion*, 9(3):482–488, 1994.

[9] Akyildiz, I.Wang, and W.Wang. Wireless mesh networks: A survey. *Elsevier Computer Networks*, 2005.

[10] P. Gupta and P. R. Kumar. The capacity of wireless networks. *IEEE Transactions on Information Theory*, 46:388–404, 2000.

[11] Richard Draves, Jitendra Padhye, and Brian Zill. Comparison of routing metrics for static multi-hop wireless networks. *Proceedings of Applications, technologies, architectures, and protocols for computer communications*, pages 133–144, 2004.

[12] Michael R. Garey and David S. Johnson. *Computers and Intractability: A Guide to the Theory of NP-Completeness.* W. H. Freeman & Co., New York, NY, USA, 1990.

[13] Dorit S. Hochba. Approximation algorithms for np-hard problems. *SIGACT News*, 28(2):40–52, 1997.

[14] J. A. Stine. Exploiting smart antennas in wireless mesh networks using contention access. *IEEE transactions on Wireless Communications*, 13:38–49, 2006.

[15] N. S. Fahmy, T. D. Todd, and V. Kezys. Ad hoc networks with smart antennas using IEEE 802.11-based protocols. *IEEE International Conference on Communications, ICC*, 5:3144–3148, 2002.

[16] N. S. Fahmy and T. D. Todd. A selective CSMA protocol with cooperative ring for ad hoc networks with smart antennas. *IEEE Wireless Communications and Networking Conference, WCNC*, 1:387–392, 2004.

[17] S.-L. Wu, C.-Y Lin, Y.-C. Tseng, and J.-P. Sheu. A New Multi-Channel MAC Protocol with On-Demand Channel Assignment for Multi-Hop Mobile Ad Hoc Networks. *Proceedings of the International Symposium on Parallel Architectures, Algorithms and Networks*, page 232, 2000.

[18] Mansoor Alicherry, Randeep Bhatia, and Li (Erran) Li. Joint channel assignment and routing for throughput optimization in multi-radio wireless mesh networks. *Proceedings of the 11th annual international conference on Mobile computing and networking*, pages 58–72, 2005.

[19] Jungmin So and Nitin H. Vaidya. Multi-channel mac for ad hoc networks: handling multi-channel hidden terminals using a single transceiver. *Proceedings of the 5th ACM international symposium on Mobile ad hoc networking and computing*, pages 222–233, 2004.

[20] Ashish Raniwala, Kartik Gopalan, and Tzi cker Chiueh. Centralized channel assignment and routing algorithms for multi-channel wireless mesh networks. *SIGMOBILE Mob. Comput. Commun. Rev.*, 8(2):50–65, 2004.

[21] Saumitra M. Das, Himabindu Pucha, Dimitrios Koutsonikolas.Y, Charlie Hu, and Dimitrios Peroulis. Dmesh: Incorporating practical directional. antennas in multi-channel wireless mesh networks. *IEEE Journal on Selected Areas in Communication*, 2006.

[22] Anand Prabhu Subramanian, Rupa Krishnan, Samir R.Das, and Himanshu Gupta. Minimum interference channel assignment in multi-radio wireless mesh

networks. *Technical Report*, 2006.

[23] Jinlong Zhang. Proposal of free space optical mesh network architecture for broadband access. *IEEE International Conference on Communications, ICC*, 4:2142–2145, 2002.

[24] A. S. Acampora and S. V. Krishnamurthy. A broadband wireless access network based on mesh-connected free-space optical links. *IEEE Personal Communications*, 6:62–65, 1999.

[25] S. V. Krishnamurthy and A. S. Acampora. Capacity of a multihop mesh arrangement of radio cells connected by free-space optical links. *12th IEEE International Symposium on Personal, Indoor and Mobile Radio Communications*, 2:G–49–G–54, 2001.

[26] J. Håstad. Clique is hard to approximate within $n^{1-\epsilon}$. *Proceedings of the 37th Annual Symposium on Foundations of Computer Science*, page 627, 1996.

[27] C. A. Murthy D. Bhandari and S. K. Pal. Genetic algorithm with elitist model and its convergence. *International Journal of Pattern Recognition and Artificial Intelligence*, 10:731–747, 1996.

[28] D. E. Goldberg. *Genetic Algorithm : Search, Optimization and Machine Learning*. Addison Wesley Publishing Company, Inc., New York, NY, USA, 1989.

[29] A. Farbod. Design and Resource Allocation for Solar-Powered ESS Mesh Networks. Master's thesis, McMaster University, Canada, August 2005.

[30] S. Fashandi. Realtime handoff in sustainable solar powered ESS Mesh Networks. Master's thesis, McMaster University, August 2005.

[31] L. Narvarte and E. Lorenzo. On the usefulness of stand-Alone PV Sizing Methods. *Progress in Photovoltaics: Research and Applications*, 8:391–409, 2000.

[32] F. Zhang, T. D. Todd, D. Zhao, and V. Kezys. Power Saving Access Points for IEEE 802.11 Wireless Network Infrastructure. In *IEEE Wireless Communications and Networking Conference, WCNC*, March 2004.

[33] L. L. Bucciarelli. The effect of day-to-day correlation in solar radiation on the probability of loss of power in a stand-alone photovoltaic energy system. *Solar Energy*, 36(1):11–14, 1986.

[34] F.M. Safie. Probabilistic modeling of solar power systems. In *Annual Proceedings Reliability and Maintainability Symposium*, pages 425–430, 1989.

[35] H.A.M. Maghraby, M.H. Shwehdi, and G.K. Al-Bassam. Probabilistic assessment of photovoltaic (PV) generation system. *IEEE Transactions on Power Systems*, 17(1):205–208, 2002.

[36] Y. Li, T. D. Todd, and D. Zhao. Access Point Power Saving in Solar/Battery Powered IEEE 802.11 ESS Mesh Networks. In *The Second International Conference on Quality of Service in Heterogeneous Wired/Wireless Networks (QShine)*, August 2005.

[37] D.L.Begley. Laser cross-link systems and technology. *IEEE Transactions on Power Systems*, 38(8):126–132, August 2000.

[38] N.Karafolas and S.Baroni. Optical satellite networks. *IEEE transactions on Lightwave Technology*, 18(12):1792–1806, December 2000.

[39] K.Wilson and M.Enoch. Optical communications for deep space missions. *IEEE Communication Magazine*, 38(8):134–139, August 2000.

[40] J.E. Mulholland and S.A. Cadogan. Intersatellite laser crosslinks. *IEEE Transactions on Aerospace and Electronic Systems.*, 32(3):1011–1020, July 1996.

[41] I.I. Kim, B.McArthur, and E.Korevaar. Comparison of laser beam propagation at 785 nm and 1550 nm in fog and haze for optical wireless communications. *Optical Wireless Communications III,SPIE*, 4214:26–37, 2001.

[42] OSRAM Opto Semiconductors. High Power Infrared Emitter, Part No. SFH4301 . http://www.osram-os.com/.

[43] Maxim Integrated products. 270 Mbps SFP LED Driver, Part No. MAX3967 . http://www.maxim-ic.com/ .

[44] Maxim Integrated products. 155 Mbps Low-Noise Transimpedance Amplifier, Part No.MAX3657 . http://www.maxim-ic.com/ .

[45] PerkinElmer Optoelectronics. Silicon PIN photodiode-Standard N-Type,Part No. C30808E . http://optoelectronics.perkinelmer.com .

[46] Maxim Integrated products. +3.0V to +5.5V, 125Mbps to 266Mbps Limiting Amplifiers with Loss-of-Signal Detector,Part No. MAX3964A . http://www.maxim-ic.com/ .

[47] HPWREN: High Performance Wireless Research and Education Network. http://hpwren.ucsd.edu/solar.htmlh/. University of California, San Diego, CA.

[48] Nortel Networks. http://www.nortelnetworks.com, 2007.

[49] MeshDynamics Inc. http://www.meshdynamics.com, 2007.

[50] BelAir Networks Inc. http://www.belairnetworks.com, 2007.

[51] Mesh Networks (Motorola Inc.). http://www.meshnetworks.com, 2007.

[52] SolarMESH Networks. http://owl.mcmaster.ca/ todd/SolarMESH/, 2007.

[53] MuniWireless. http://www.muniwireless.com/, 2007.

[54] S.Arnon and S.Kopeika. Laser satellite communication network – vibration effect and possible solutions. *Proceedings of the IEEE*, 85(10):1646–1661, October 1997.

[55] S.Bloom, E.Korevaar, J.Schuster, and H.Willebrand. Understanding the performance of free-space optics. *OSA Journal of Optical Networking*, 4214:178–200, June 2003.

[56] Hamid Hemmati Ed. *Deep Space Optical Communications.* Wiley Inter-Science, Hoboken, NJ, USA, 2006.

[57] S. Gagliano, S. Raiti, and G. Tina (Italy). Unit Sizing Probabilistic Optimal of a Grid-Linked Hybrid Solar/Wind Power System. *Power and Energy Systems*, page 468, 2005.

[58] Yuichi Tanaka. *A study on Optical Wireless Communication Systems and their Applications.* PhD thesis, Keio University, March 2002.

[59] Cordeiro M.C.R, Colvero C.P, and von der Weid J.P. Experimental comparison of scintillation effects in far and near infrared wavelengths in FSO systems. In *IEEE International Conference on Microwave and Optoelectronics*, July 2005.

[60] Igor I. Smolyaninova, Linda Wasiczko, Kyuman Cho, and Christopher C. Davis. Long-distance 1.2 Gb/s optical wireless communication link at 1550nm. *Free-Space Laser Communication and Laser Imaging,SPIE*, 4489:241–250, 2002.

[61] Heatley D.J.T, Wisely D.R., and Neild I.and Cochrane P. Optical wireless: the story so far. *IEEE Communications Magazine*, 36:72–74,79–82, December 1998.

[62] Haiping Wu, Bela Hamzeh, and Mohsen Kavehrad. Achieving carrier class availability of FSO link via a complementary RF link. *Conference on Signals, Systems and Computers*, 2:1483–1487, 2004.

[63] Eric J. Korevaar. Solar background effects in wireless optical communications. *Proceedings of SPIE, Optical Wireless Communications*, pages 133–142, December 2002.

[64] American National Standards Institute (ANSI). *Standard for the Safe Use of Lasers.* ANSI Z136.1, http://www.ansi.org.

[65] International Electrotechnical Commission (IEC). *Safety of Laser Products Part 1: Equipment Classification, Requirements, and Users Guide, IEC 825-1.* Published in 1993 and amended in 1997, the standard is being redesignated as IEC 60825-1,http://www.iec.ch.